Typeset using LaTeX **twocolumn** style in AASTeX63

Draft version March 2, 2021

SED Analysis of 43 Spectroscopically Confirmed Galaxies at z ≃ 6 to Constrain Possible Relationships between UV Slope, Model Dust Attenuation, and Escape Fraction

Junehyoung Jeon,[1] Rogier A. Windhorst,[1] Seth H. Cohen,[1] Rolf A. Jansen,[1] Brent M. Smith,[1] Timothy Carleton,[1] Eiichi Egami,[2] Kristian Finlator,[3] and Linhua Jiang[4]

[1] *School of Earth & Space Exploration, Arizona State University, Tempe, AZ 85287-1404, USA*
[2] *Steward Observatory, University of Arizona, 933 North Cherry Avenue, Tucson, AZ 85721, USA*
[3] *New Mexico State University, Las Cruces, NM 88003, USA*
[4] *Kavli Institute for Astronomy and Astrophysics, Peking University, Beijing 100871, China*

ABSTRACT

The reionization of the Universe is thought to have completed by redshift $z \simeq 5.5$. To probe this era, galaxy observations in the Subaru Deep Field (SDF) have identified more than 100 galaxies at $z \simeq 6$, many spectroscopically confirmed through follow-up observations. **Using available optical/IR data, we model with CIGALE the spectral energy distributions (SEDs) of 43 SDF galaxies, including newly acquired data from the UKIRT WFCAM K-band for seven previously studied objects.** In particular, modeling deep IR photometry is sensitive to the galaxy's Lyman continuum (LyC) escape fraction ($f_{\rm esc}$). We find the **median implied $f_{\rm esc}$ value as ∼0.4±0.1 (mean error). Significant uncertainties in data and fitting result in a large range of $f_{\rm esc}$ for individual objects, but analysis suggests that $f_{\rm esc}$ is likely high enough for galaxies to finish reionization by $z \sim 6$.** More importantly, we find trends between the CIGALE UV slope β, $f_{\rm esc}$, and dust extinction $E_{\rm B-V}$: for a given $E_{\rm B-V}$, β **appear steeper by ∼0.4 than at $z = 0$.** Lower $f_{\rm esc}$ values appear to be associated with bluer β and lower $E_{\rm B-V}$, **but only weakly. This suggests that** LyC could have escaped through holes with sufficiently wide opening angles surrounding the ISM from outflows of supernovae and/or weak AGN **to escape, but resulting in a large range of implied $f_{\rm esc}$ values depending on the orientation of each galaxy. The current *HST*, *Spitzer* and ground-based photometric and model errors for the 43 galaxies are large, so IR spectroscopic observations with the *James Webb Space Telescope* are needed to better constrain this possibility.**

Keywords: High-Redshift Galaxies — Spectral Energy Distributions — Interstellar Dust Extinction — Reionization

1. INTRODUCTION

Detailed studies of high redshift galaxies observed in the first billion years have provided a wealth of information about early galaxy formation and evolution. Developments in ground- and space-based telescopes, such as the availability of very wide-field cameras on 8 to 10m class telescopes and medium- or narrow-band filters that fall between the worst sky lines, enabled the identification of numerous high redshift galaxies (*e.g.*, Jiang et al. 2013; Finkelstein et al. 2019). The planned *James Webb Space Telescope (JWST)*, which can access wavelengths presently inaccessible with *Hubble Space Telescope (HST)* and difficult to access from the ground due to Earth's atmosphere, will be able to observe these objects at higher resolution to identify AGN, star-formation regions, and outflows (*e.g.*, Gardner et al. 2006; Maseda et al. 2019; Windhorst et al. 2018). In particular, observations with the Subaru telescope, *HST*, and the *Spitzer Space Telescope* have discovered numerous high redshift galaxies in optical, near-IR, and mid-IR, respectively (*e.g.*, McLure et al. 2011; Kashikawa et al. 2011; Trenti et al. 2011). Large areas of sky have been imaged from the ground with narrow-band filters, and the detected narrow-band emission of some of the brighter galaxies was spectroscopically confirmed to be Lyman α (Lyα) emission (*e.g.*, Jiang et al. 2013, 2016).

Corresponding author: Junehyoung Jeon
jjeon20@asu.edu

As the reionization of the early universe is thought to have been completed by $z \simeq 5.5$ (*e.g.*, Keating et al. 2020), such high redshift galaxies can help us study this period.

Some parameters of these high redshift galaxies useful for studying the epoch of reionization are their UV-continuum slope (β), which can help constrain the characteristics of their young stellar populations such as their age (Jiang et al. 2020), their Lyman Continuum (LyC) escape fraction ($f_{\rm esc}$) which provides a measure of how much energy was available for reionization (*e.g.*, Miralda-Escudé et al. 2000; Loeb & Barkana 2001; Barrow et al. 2020), and the $E_{\rm B-V}$ reddening values (*e.g.*, Calzetti et al. 2000; Meurer et al. 1999) which are a measure of their internal attenuation by dust. Notably, $E_{\rm B-V}$ or β may be correlated with $f_{\rm esc}$, given that β is related to the amount of ionizing emission originating from the galaxy and $E_{\rm B-V}$ is related to the amount of dust and gas preventing that emission from escaping the galaxy (*e.g.*, Ono et al. 2010; Hayes et al. 2011).

Previous studies have suggested that a minimum escape fraction of ∼20% is needed to finish the reionization of the Universe at $z \simeq 6$ **when UV-bright sources dominate ($M_{AB} \lesssim -21$) (*e.g.*, Finkelstein et al. 2019; Naidu et al. 2020)**. However, it is unclear what $f_{\rm esc}$ values are typical for $z \simeq 6$ galaxies.

Using photometric methods, several authors found unusually blue β values as steep as $\beta \simeq -2 \sim -3$ for faint galaxies at $z \geq 6$ (*e.g.*, **Bouwens et al. 2014; Labbé et al. 2010; Jiang et al. 2020**). To see how such surprisingly blue slope parameters might occur, SED modeling — which previously has been used to characterize galaxy populations at low (Papovich et al. 2001; Shapley et al. 2001, 2005) and moderate redshifts (Ono et al. 2010) — can be used to measure the UV slope β. As nebular emission **is crucial in producing accurate SED models (*e.g.*, Schaerer & de Barros 2009; Jiang et al. 2016) – for significant nebular emission indicates that the LyC excites the gas to produce rest-frame optical emission lines instead of escaping, reducing the implied $f_{\rm esc}$ – SED modeling can be used to constrain the amount of ionizing emission originating from galaxies.**

To perform such modeling of a large number of galaxies in the Subaru Deep Field (SDF), 67 candidate galaxies at $z \simeq 6$ were identified in Jiang et al. (2013)[1]. These galaxies were identified to be the most luminous galaxies in Lyα emission and/or in UV-continuum in this redshift range around $z \simeq 6$. Of these galaxies, 7 **galaxies chosen to have particularly blue** β were imaged by *HST* Wide Field Camera 3 (WFC3) in the F105W, F110W, F125W, F140W, and F160W filters, and their rest-frame UV SEDs were modeled with the CIGALE program (Boquien et al. 2019), as described in detail in Jiang et al. (2020, hereafter J20).

Of these 7 galaxies, 6 **had observed *HST* photometry that indicated** extremely blue β ($\beta \lesssim -2.5$), which presents a challenge to stellar population synthesis models, as the galaxies can yield such blue slopes only under the assumption of extremely young ages and low metallicities. We refer to these seven galaxies of J20 as the **"7 galaxies of J20" throughout the text**.

In this paper, we study the SEDs of these 7 galaxies of J20, as well as 36 additional galaxies with available near-IR data out of 67, and compare these samples. Our goal for this comparison is to determine if, and to what extent, galaxy parameters are correlated with LyC escape fraction, and how galaxy properties are related to the slope of the UV continuum. We use the CIGALE code for our SED models, which was also used by J20 for the 7 galaxies. For all 43 SDF galaxies, we not only fit the stellar age, but also explore the values of the LyC escape fraction ($f_{\rm esc}$) and dust extinction ($E_{\rm B-V}$) allowed for each galaxy to determine their best SED fit. This paper thus presents the SED models of the 43 $z \simeq 6$ galaxies in the SDF that have suitable near-IR data to possibly constrain their escape fraction, and discusses the range of SED parameter values permitted by the CIGALE models for each of these galaxies.

The paper is organized as follows. In section 2, we describe all available data for these $z \simeq 6$ galaxies, and add archival UKIRT/WFCAM K-band data in the analysis of **the 7 galaxies of J20**. In section 3, **we describe how the SED modeling of the galaxies was performed, and describe the results.** In section 4, we discuss the implications of the SED models of the 7 galaxies of J20. In section 5, we discuss constraints to the implied $f_{\rm esc}$, β, and $E_{\rm B-V}$ values for the full sample of 43 SDF galaxies at $z \simeq 6$ and investigate possible trends. We then summarize our final results in section 6. All AB magnitudes from J20 are converted to mJy to facilitate direct modeling with the CIGALE program (Oke & Gunn 1983).

2. OVERVIEW OF EXTANT GALAXY DATA USED

Table 1 lists IDs, coordinates, redshifts, and measured fluxes of the 43 galaxies in our sample as given in Jiang et al. (2013, 2016) and J20. **We also include**

[1] Five of the spectroscopically confirmed galaxies are not in the SDF, but rather the UKIDSS Ultra-Deep Survey (UDS), with WFC3-IR coverage from the Cosmic Assembly Near-infrared Deep Extragalactic Legacy Survey (CANDELS; Grogin et al. 2011; Koekemoer et al. 2011).

the UV-slope measurements for the 7 galaxies of J20 (ID07, ID28, ID30, ID43, ID61, ID63, ID64). *HST*/WFC3 images in the F105W, F110W, F125W, F140W, and/or F160W filters are available in various combinations for all **43** galaxies, and a subset of our sample also has *Spitzer*/IRAC imaging available **in the SDF or from the larger area covered by the Subaru XMM-Newton Deep Survey (Furusawa et al. 2008) from Jiang et al. (2013, 2016). Sub-pixel dithering was performed to improve the Point Spread Function (PSF) sampling (Jiang et al. 2013). For the optical *HST* images, photometry was performed using SExtractor (Bertin & Arnouts 1996) adopting a 2″ diameter circular aperture and subtracting the local background. We applied an aperture correction based on bright point sources within the same image to account for any light losses outside each object aperture. PSFs were matched through weight maps proportional to the inverse square of the PSF Full Width at Half Maximum (FWHM), instead of homogenizing the PSFs to a certain value. For the infrared images, SExtractor was used with a Kron factor of 1.8 to determine the total magnitudes with aperture corrections as well. For the IRAC 3.6 and 4.5 μm data, deblending was first done by modeling the brightest neighbors of the source with iGALFIT (Ryan 2011), convolving with the PSF image, and then subtracting the neighbors from the image. Photometry was then done on a 1″.8 radius aperture with an aperture correction of 0.4 mag (Jiang et al. 2016).**

Since CIGALE provides SED models into the observed infrared regime, we searched the *Herschel* archive for images of the 7 galaxies to possibly constrain their dust content. In the region of the SDF containing our 43 galaxies, extant *Herschel* far-IR observations are too shallow for robust detections of any of our sample galaxies. Hence, **we have no far-IR data to place further constraints on thermal dust emission in our CIGALE modeling.**

Deep observations as part of the UKIRT WFCAM Large Area Survey (LAS) or the Ultra Deep Survey (UDS) (Lawrence et al. 2007) observed the 7 SDF galaxies of J20 in the K-band, and provided 2.2 μm flux measurement or upper limits. In those cases, the 7 galaxies have 5–6 independent flux measurements, in addition to K-band observations, which helps better constrain the range of implied physical parameters allowed by the CIGALE models. For the 60 remaining SDF galaxies not analyzed by J20, 14 galaxies did not have any reliable flux measurements. An additional 6 galaxies only had one reliable flux measurement, so they were also omitted. **Finally, we also omitted 4 galaxies that had neither K-band nor IRAC measurements — *i.e.*, no measurements beyond 2 μm— and thus did not allow meaningful modeling of their escape fractions. The K-band data was not used for these galaxies, since it did not improve the modeling of the 7 galaxies significantly.** Thus, 43 galaxies could be modeled by CIGALE out of the full sample of 67 SDF galaxies.

To obtain the K-band data for the 7 galaxies of J20, we searched the WFCAM Science Archive[2]. After identifying the exposures containing each of the 7 galaxies, we used DS9 (Joye & Mandel 2003) to analyze the K-band image files. We selected a region around the location of each galaxy and a region of background sky devoid of object signal to estimate the source and background flux measurements on the Vega system, given the zero-point of Hodgkin et al. (2009). **The pixel numbers in the regions were used to measure the flux, and the standard deviation of the background pixel values was used to estimate the uncertainties in the measured flux values.** For the K-band, we used the conversion from Vega to AB magnitudes from Hewett et al. (2006). We converted the apparent AB-magnitude values to μJy units (Oke & Gunn 1983).

Except for ID63 and ID64 observed in the UDS field, the remainder of the galaxies were observed in the UKIRT WFCAM LAS with shallower observations. A 2σ upper limit to the K-band fluxes is therefore listed for five galaxies in Table 1, which in a few cases still provides a meaningful additional constraint to the CIGALE SED model fits.

[2] http://wsa.roe.ac.uk/

Table 1. High redshift galaxy data with measured UV slope from J20

ID	R.A.	Decl.	z	Slope	z'	y'	F105W	F110W	F125W	F140W	F160W	IRAC 1	IRAC 2	K
	J2000.0	J2000.0		β	μJy	μJy	μJy	μJy	μJy	μJy	μJy	μJy	μJy	μJy
(1)	(2)	(3)	(4)	(5)	(6)	(7)	(8)	(9)	(10)	(11)	(12)	(13)	(14)	(15)
ID07	13:24:15.987	+27:16:11.05	5.691	-3.38 ± 0.35	0.116 ± 0.015	0.073 ± 0.018	0.079 ± 0.01	...	0.073 ± 0.008	...	0.052 ± 0.008	...	...	<0.173
ID28	13:24:42.452	+27:24:23.35	6.042	-2.57 ± 0.20	0.200 ± 0.011	...	...	0.129 ± 0.010	..	0.110 ± 0.011	0.100 ± 0.009	0.211 ± 0.076	...	<0.103
ID30	13:24:00.301	+27:32:37.95	6.062	-2.60 ± 0.25	0.187 ± 0.012	0.131 ± 0.016	0.194 ± 0.016	...	0.153 ± 0.015	...	0.139 ± 0.017	0.229 ± 0.074	...	<0.279
ID43	13:23:53.054	+27:16:30.75	6.542	-3.39 ± 0.41	0.102 ± 0.012	0.139 ± 0.027	0.152 ± 0.018	...	0.111 ± 0.007	...	0.087 ± 0.009	0.275 ± 0.061	...	<0.263
ID61	13:25:22.291	+27:35:19.95	6.599	-1.41 ± 0.30	0.092 ± 0.001	0.215 ± 0.020	0.142 ± 0.012	...	0.143 ± 0.016	...	0.158 ± 0.010	0.847 ± 0.055	0.575 ± 0.095	<0.321
ID63	02:18:00.899	−05:11:37.69	6.027	-2.89 ± 0.16	0.466 ± 0.026	0.360 ± 0.050	0.270 ± 0.037	...	0.305 ± 0.014	...	0.247 ± 0.018	0.581 ± 0.065	0.373 ± 0.086	0.275 ± 0.003
ID64	02:17:35.337	−05:10:32.50	6.120	-2.77 ± 0.15	0.331 ± 0.018	0.296 ± 0.049	0.244 ± 0.029	...	0.261 ± 0.016	...	0.192 ± 0.012	0.398 ± 0.040	...	0.258 ± 0.033
ID02	13:23:54.601	+27:24:12.72	5.654	...	0.095±0.012	0.111±0.028	...	0.052±0.005	0.055±0.006	...	0.051±0.006	0.066±0.012	...	...
ID03	13:24:16.468	+27:19:07.65	5.665	...	0.331±0.012	0.353±0.026	...	0.291±0.011	...	...	0.286±0.018	0.334±0.065	0.254±0.077	...
ID05	13:24:11.887	+27:41:31.81	5.681	...	0.100±0.012	0.082±0.027	...	...	0.069±0.007	...	0.060±0.009	0.080±0.015	...	...
ID10	13:24:33.097	+27:29:38.58	5.696	...	0.062±0.006	0.081±0.015	...	...	0.052±0.017	...	0.040±0.005	0.105±0.022	...	...
ID15	13:24:23.705	+27:33:24.82	5.710	...	0.492±0.014	0.461±0.025	...	0.501±0.014	...	...	0.409±0.023	0.879±0.057	0.698±0.071	...
ID20	13:24:40.527	+27:13:57.91	5.724	...	0.119±0.012	0.113±0.028	...	...	0.139±0.012	...	0.138±0.014	0.302±0.083	...	...
ID21	13:24:30.633	+27:29:34.61	5.738	...	0.084±0.010	...	...	...	0.049±0.006	...	0.048±0.008	0.125±0.023	...	...
ID22	13:24:41.264	+27:26:49.09	5.743	...	0.077±0.011	...	...	...	0.069±0.011	...	0.069±0.013	0.097±0.018	...	...
ID23	13:24:18.450	+27:16:32.56	5.922	...	0.244±0.011	0.198±0.025	...	...	0.213±0.010	...	0.201±0.013	0.328±0.048	...	...
ID24	13:25:19.463	+27:18:28.51	6.002	...	0.244±0.011	0.198±0.025	...	0.213±0.010	...	...	0.201±0.013	0.328±0.048	...	...
ID25	13:24:26.559	+27:15:59.72	6.032	...	0.291±0.013	0.281±0.026	...	0.164±0.018	...	...	0.209±0.021	0.692±0.045	0.592±0.071	...
ID27	13:24:10.766	+27:19:03.95	6.040	...	0.086±0.012	...	...	...	0.098±0.010	...	0.069±0.012	0.191±0.053	...	...
ID29	13:24:05.895	+27:18:37.72	6.049	...	0.058±0.011	...	...	...	0.045±0.005	...	0.042±0.007	0.086±0.016	...	...
ID33	13:24:20.628	+27:16:40.47	6.269	...	0.081±0.012	...	...	...	0.070±0.008	...	0.064±0.010	0.082±0.015	...	...
ID34	13:23:45.757	+27:32:51.30	6.315	...	0.219±0.012	0.350±0.026	...	...	0.398±0.015	...	0.398±0.015	0.108±0.089	...	...
ID36	13:23:45.937	+27:25:18.06	6.482	...	0.189±0.012	0.265±0.029	...	0.182±0.012	...	...	0.192±0.014	0.363±0.064	0.302±0.078	...
ID37	13:24:18.416	+27:33:44.97	6.508	...	0.077±0.012	0.086±0.027	...	0.071±0.010	...	...	0.068±0.018	0.082±0.015	...	...
ID40	13:24:55.772	+27:40:15.31	6.534	...	0.040±0.012	0.128±0.028	...	...	0.077±0.008	...	0.046±0.011	0.084±0.015	...	...
ID44	13:24:15.678	+27:30:57.79	6.543	...	0.227±0.010	0.331±0.015	...	...	0.325±0.015	...	0.366±0.020	1.127±0.052	0.895±0.074	...
ID47	13:24:10.817	+27:19:28.08	6.547	...	0.121±0.011	0.356±0.026	...	...	0.501±0.014	...	0.492±0.018	1.202±0.055	1.159±0.097	...
ID49	13:24:17.909	+27:17:45.94	6.548	...	0.047±0.013	0.097±0.029	...	...	0.108±0.010	...	0.105±0.013	0.268±0.059	...	...
ID50	13:23:44.896	+27:31:44.90	6.550	...	0.104±0.012	0.113±0.024	...	...	0.076±0.008	...	0.082±0.011	0.545±0.080	...	...
ID54	13:24:08.313	+27:15:43.49	6.556	...	0.163±0.012	0.219±0.026	...	...	0.150±0.019	...	0.171±0.024	0.319±0.073	0.299±0.010	...
ID58	13:24:43.427	+27:26:32.62	6.583	...	0.082±0.011	0.184±0.029	...	...	0.179±0.015	...	0.192±0.018	0.242±0.058	0.470±0.010	...
ID62	13:23:59.766	+27:24:55.75	6.964	...	0.058±0.016	0.394±0.033	...	0.229±0.008	0.247±0.011	...	0.242±0.011	0.421±0.062	0.310±0.060	...
ID67	02:17:57.585	-05:08:44.72	6.595	...	0.171±0.024	0.353±0.049	...	...	0.437±0.038	...	0.437±0.032	1.180±0.043	0.724±0.053	...
ID04	13:24:32.885	+27:30:08.82	5.671	...	0.278±0.013	0.273±0.035	...	...	0.133±0.013	...	0.134±0.017	0.445±0.090	...	...
ID17	13:23:44.747	+27:24:26.81	5.716	...	...	...	...	...	0.065±0.008	...	0.025±0.005	0.086±0.016	...	...
ID31	13:23:45.632	+27:17:00.53	6.112	...	0.334±0.012	...	...	0.116±0.015	...	...	0.100±0.017	0.344±0.063	...	...
ID35	13:24:40.643	+27:36:06.94	6.332	...	0.219±0.012	...	...	...	0.240±0.013	...	0.225±0.015	1.854±0.09	1.159±0.117	...
ID39	13:23:43.190	+27:24:52.04	6.534	...	0.071±0.013	...	...	...	0.084±0.010	...	0.090±0.012	0.097±0.018	...	...
ID45	13:24:40.239	+27:25:53.11	6.544	...	...	...	...	...	0.059±0.010	...	0.044±0.012	0.101±0.019	...	...
ID46	13:23:52.680	+27:16:21.76	6.545	...	...	...	...	...	0.077±0.009	...	0.079±0.012	0.102±0.019	...	...
ID48	13:23:48.922	+27:15:30.33	6.548	...	...	...	...	...	0.048±0.008	...	0.047±0.011	0.105±0.019	...	...
ID52	13:24:35.005	+27:39:57.43	6.554	...	0.043±0.012	...	...	...	0.034±0.005	...	0.031±0.006	0.0.093±0.017	...	...
ID66	02:18:20.701	−05:11:09.89	6.575	...	...	...	...	...	0.074±0.014	...	0.077±0.016	0.158±0.047	...	...

NOTE—The ID numbers are from Table 1 in Jiang et al. (2013). The z'- and y'-band fluxes are from Jiang et al. (2013), and the remainder from Jiang et al. (2016, 2020). The β values are also from J20. Some galaxies do not have measurements in some of the filters, so those columns are left empty. For the K-band data, the first five galaxies are not detected at 3σ, so 2σ upper limits are given. **The last 10 galaxies did not have any data below the Balmer break and so were set apart.**

3. SED MODELING

The Lyman-continuum escape fraction ($f_{\rm esc}$) may be constrained by the implied presence of emission lines in the SED of galaxies. A stellar population produces a certain number of ionizing photons based on its age and stellar mass. If none of those photons escape ($f_{\rm esc}$=0), then the energy will be reprocessed in the ISM, producing strong emission lines. If the escape fraction is high ($f_{\rm esc}\gtrsim$0.3), there will be no associated emission lines (e.g., Smith et al. 2018, 2020; Steidel et al. 2018). CIGALE uses the modeled stellar age and stellar mass to determine the expected emission line strength, which may be many Angstroms in equivalent width for these very young stellar populations, and predicts the associated emission line strengths for a given $f_{\rm esc}$ value. If the near-IR photometry at the emission line wavelengths is brighter than the CIGALE models predict, then the presence of stronger emission line is implied, suggesting lower $f_{\rm esc}$ values, and vice-versa. Ultimately, because of uncertainties in the measured stellar population parameters, near-IR photometry is only weakly dependent on $f_{\rm esc}$, resulting in larger errors in the implied $f_{\rm esc}$ values. However, deep multi-band photometry including the *Spitzer* IRAC 3.6–4.5 μm images can place some meaningful constraints on the allowed $f_{\rm esc}$-values for these 43 galaxies, enabling us to explore the average $f_{\rm esc}$-value range for galaxies at this redshift, and search for any trends that may exist between $f_{\rm esc}$ and other galaxy properties.

We so used the CIGALE program (Boquien et al. 2019) to perform SED modeling for all our SDF galaxies. We also used the broadband fluxes from Jiang et al. (2016, 2020) for CIGALE fitting, as described in § 2. Following J20, we sampled the model ages between **10 to 800 Myr using a fixed log scale** for redshifts $z > 6.0875$ and $z < 6.0875$, respectively, so as to not exceed the age of the Universe at each redshift. We sampled the escape fraction from 0 to 1 in steps of 0.1. The metallicity values sampled were 0.0001, 0.0004, 0.004, 0.008, 0.02, and 0.05. The $E_{\rm B-V}$ values we sampled were between 0 and **0.7** mag using a Calzetti et al. (2000) extinction curve. AGN models were not tested since no significant change was observed in the models by allowing the presence of a weak AGN in J20.

In the modeling, the dust extinction law of Calzetti et al. (2000) was considered. A discussion of the possible evolution in metallicity and dust extinction is given by *e.g.*, Kim et al. (2017). Smith et al. (2020) and Oesch et al. (2013), suggesting that SMC extinction curves may provide a better fit to the SED of star-forming galaxies at $z \simeq 2.3-3.5$. However, we found no significant change in the best-fit SED models when using the SMC extinction curve instead for our SDF sample at $z \simeq 6$.

Most galaxy models showed ages greater than 100 Myr and small values of extinction, which is consistent with the results of Jiang et al. (2016), where the SED models were done with GALEV (Kotulla et al. 2009). Fig. 1 presents the SED models of all 43 galaxies.

Rather than reporting the best-fit values from this analysis, which do not capture uncertainties associated with this fitting, we report Bayesian average values and uncertainties associated with each parameter, as described in Noll et al. (*e.g.*, 2009). CIGALE computes such uncertainties by taking the average value and standard deviation of the fit to be the average and standard deviation of all models, weighted by the p-value associated with the model's χ^2 value. These values give a much more comprehensive picture of the fit than only the best-fit values.

One potential concern related to our SED modeling is whether objects with observations in only one IRAC band still allow meaningful measurements of $f_{\rm esc}$ with our method. To test this, we investigated the 11 objects with observations in both IRAC bands. For these objects, we modeled the SEDs both including and excluding the 4.5 μm band photometry. The results of this are shown in Tables 2 and 3, as well as Fig. 2. Because of the large uncertainties in the 4.5 μm band photometry, excluding it in the modeling did in general not significantly affect the inferred model parameters. More than half the galaxies for each parameter overlapped in the values for the two sets of models. Thus, we kept the objects with only 3.6 μm observations in our final sample. We apply a similar procedure to test the impact of the inclusion of K-band data in the 7 galaxies from J20, with the results shown in Tables 4 and 5. Again, the inclusion of K-band data does not significantly bias the results, so the inclusion of galaxies without K-band data is warranted.

To demonstrate that this fitting is sensitive to the escape fraction, Fig. 3 illustrates an SED fit to objects ID43 and ID63 with a fixed $f_{\rm esc}$ value of 1. The resulting fits have clearly higher χ^2 values, failing to reproduce the observed steep β and underestimating the 3.6 μm flux. In addition, we directly tested how χ^2 depends on escape fraction using the Pearson correlation test. Fig. 4 and 5, which present the model param-

Table 2. Best-fit parameters and χ^2 values of the 11 galaxies using both IRAC bands

ID	Reduced χ^2	Slope	Metallicity	Age	Escape fraction	$E_{\rm B-V}$
		β	Z	Myr		mag
(1)	(2)	(3)	(4)	(5)	(6)	(7)
ID03	0.29	−2.39±0.17	0.007±0.011	111±129	0.53±0.31	0.2±0.11
ID15	0.16	−2.23±0.14	0.0067±0.0082	372±280	0.41±0.32	0.2±0.12
ID25	3.43	−2.11±0.13	0.0056±0.0046	537±134	0.12±0.17	0.1±0.09
ID35	5.15	−1.20±0.15	0.007±0.009	505±123	0.39±0.31	0.5±0.08
ID36	0.67	−2.10±0.22	0.010±0.013	248±213	0.49±0.31	0.0±0.16
ID44	0.29	−1.66±0.20	0.009±0.011	271±223	0.36±0.30	0.5±0.15
ID47	0.45	−1.54±0.21	0.012±0.015	180±185	0.48±0.31	0.7±0.15
ID54	0.50	−2.06±0.27	0.011±0.017	244±215	0.47±0.31	0.0±0.18
ID58	0.19	−1.92±0.27	0.011±0.017	163±188	0.49±0.32	0.5±0.19
ID62	1.21	−2.24±0.19	0.012±0.016	277±202	0.51±0.31	0.0±0.14
ID67	1.10	−1.00±0.20	0.008±0.009	112±166	0.23±0.26	0.4±0.13

NOTE—The model parameters along with their Bayesian error ranges of the 11 galaxies with both IRAC bands included in the fitting.

Table 3. Best-fit parameters and χ^2 values of the 11 galaxies with both IRAC bands modeled without IRAC2 at 4.5μm

ID	Reduced χ^2	Slope	Metallicity	Age	Escape fraction	$E_{\rm B-V}$
		β	Z	Myr		mag
(1)	(2)	(3)	(4)	(5)	(6)	(7)
ID03	0.25	−2.34±0.29	0.006±0.011	143±173	0.49±0.31	0.3±0.13
ID15	0.16	−2.23±0.14	0.0067±0.0082	372±280	0.41±0.32	0.2±0.12
ID25	4.19	−2.16±0.16	0.006±0.005	511±167	0.11±0.16	0.1±0.10
ID35	2.60	−1.03±0.09	0.007±0.006	579±63	0.37±0.30	0.7±0.03
ID36	0.87	−2.07±0.25	0.009±0.012	245±215	0.48±0.31	0.7±0.03
ID44	0.09	−1.54±0.20	0.009±0.012	352±213	0.44±0.32	0.3±0.14
ID47	0.42	−1.51±0.21	0.011±0.015	203±191	0.48±0.31	0.7±0.14
ID54	0.66	−2.08±0.30	0.011±0.015	224±211	0.46±0.31	0.0±0.18
ID58	0.00	−2.09±0.29	0.014±0.018	135±164	0.51±0.31	0.1±0.18
ID62	1.35	−2.21±0.20	0.012±0.015	304±213	0.52±0.31	0.0±0.14
ID67	0.78	−1.60±0.23	0.009±0.012	267±212	0.45±0.31	0.4±0.15

NOTE—The model parameters along with their Bayesian error ranges of the same 11 galaxies as in Table 2, but modeled without using the IRAC 4.5 μm band.

eters, *only* include objects for which there is a significant correlation between χ^2 and absolute value of the difference between the Bayesian $f_{\rm esc}$ and the best-fit $f_{\rm esc}$. Applying the Pearson correlation test, 14 galaxies show this correlation (we refer to those as the more reliable $f_{\rm esc}$ estimates), and the relationships between model parameters is similar to those that showed correlation between the Bayesian $f_{\rm esc}$ and the χ^2 value only, so our procedure is able to provide meaningful constraints on escape fraction of $z \sim 6$ galaxies.

Tables 4–6 show the results from a Bayesian treatment of the model parameters of Fig. 1 and list uncertainties that are critical in subsequent analysis.

Fig. 4 shows the distributions of the implied UV slope β, escape fraction $f_{\rm esc}$, and extinction values $E_{\rm B-V}$ **for the 14 galaxies with the more reliable $f_{\rm esc}$-estimates.** The $f_{\rm esc}$ and β values are the Bayesian values, **while $E_{\rm B-V}$ values are the best-fit values.**

Table 4. Best-fit parameters and χ^2 values of the 7 galaxies without using the K-band

ID	Reduced χ^2	Slope	Metallicity	Age	Escape fraction	E_{B-V}
		β	Z	Myr		mag
(1)	(2)	(3)	(4)	(5)	(6)	(7)
ID07	0.40	-2.58 ± 0.22	0.005 ± 0.010	121 ± 201	0.54 ± 0.31	0.0 ± 0.09
ID28	0.34	-2.64 ± 0.12	0.003 ± 0.005	104 ± 160	0.16 ± 0.17	0.0 ± 0.05
ID30	0.77	-2.45 ± 0.15	0.008 ± 0.012	178 ± 198	0.24 ± 0.22	0.1 ± 0.08
ID43	1.29	-2.32 ± 0.25	0.005 ± 0.007	265 ± 230	0.35 ± 0.30	0.1 ± 0.13
ID61	2.59	-1.54 ± 0.16	0.006 ± 0.007	452 ± 185	0.34 ± 0.31	0.4 ± 0.11
ID63	0.66	-2.46 ± 0.09	0.004 ± 0.003	237 ± 231	0.07 ± 0.11	0.1 ± 0.06
ID64	0.35	-2.49 ± 0.10	0.004 ± 0.003	197 ± 224	0.09 ± 0.11	0.04 ± 0.06

NOTE—The model parameters along with their Bayesian error ranges of the **7 galaxies of J20 excluding the K-band data**.

Table 5. Best-fit parameters and χ^2 values of the 7 galaxies when using the K-band

ID	Reduced χ^2	Slope	Metallicity	Age	Escape fraction	E_{B-V}
		β	Z	Myr		mag
(1)	(2)	(3)	(4)	(5)	(6)	(7)
ID07	0.60	-2.55 ± 0.23	0.005 ± 0.01	137 ± 219	0.52 ± 0.31	0.0 ± 0.10
ID28	0.27	-2.64 ± 0.12	0.003 ± 0.005	92 ± 146	0.16 ± 0.17	0.0 ± 0.05
ID30	0.64	-2.45 ± 0.15	0.008 ± 0.012	177 ± 198	0.24 ± 0.22	0.1 ± 0.08
ID43	1.04	-2.32 ± 0.25	0.005 ± 0.007	267 ± 230	0.35 ± 0.30	0.1 ± 0.13
ID61	2.17	-1.54 ± 0.16	0.006 ± 0.007	455 ± 183	0.34 ± 0.30	0.46 ± 0.11
ID63	0.75	-2.43 ± 0.08	0.004 ± 0.004	291 ± 232	0.08 ± 0.12	0.1 ± 0.06
ID64	0.70	-2.45 ± 0.09	0.004 ± 0.003	271 ± 239	0.09 ± 0.11	0.1 ± 0.06

NOTE—The model parameters along with their Bayesian error ranges of the **7 of J20 galaxies including the K-band data**.

This is because CIGALE uses the $z = 0$ slope of the E_{B-V} vs. β relation from the Calzetti et al. (2000) and Meurer et al. (1999) relations (with an intercept to be determined) to estimate E_{B-V} for a given β-value, and so deriving both E_{B-V} and β Bayesian values fully independently is not possible. The CIGALE models do imply that the intercept at $z = 6$ of the Calzetti/Meurer E_{B-V} vs. β relation at $z = 0$ needs to be ∼0.4 bluer in β than at z=0 (while adopting the same slope), and this is visible in Fig. 5a.

The cumulative Gaussian probability distributions in Fig. 4 are shown for bluer galaxies ($\beta < -2.35$) and redder galaxies ($\beta > -2.35$). The median value of the cumulative Gaussian for the $f_{esc}$is $\simeq$0.4±0.1 (mean error), but there exists a large range of values between 0-0.8. The 14 galaxies with the more reliable f_{esc}-estimates have an average f_{esc}-value with 1-sigma error range of $f_{esc}\simeq0.35^{+0.1}_{-0.2}$, which is consistent with the mean of the cumulative Gaussian distribution of the total sample of $f_{esc}\simeq$0.4±0.1 above. Regardless, the range of allowed f_{esc}-values does suggest that the CIGALE models imply escape fractions that are on average sufficiently high to reionize the Universe **with these UV-bright galaxies** (Finkelstein et al. 2019; Naidu et al. 2020). Furthermore, **it can be seen that bluer galaxies tend to have lower f_{esc} and E_{B-V} values. This trend is also seen when the galaxies are not first divided into two bins in UV slope β.**

Fig. 5 shows comparisons between model parameters for the most reliable galaxies. Fig. 5a shows the $z \simeq 0$ relation between E_{B-V} and β using the equations that Meurer et al. (1999) and Calzetti et al. (2000) found at $z \simeq 0$. The $z \simeq 6$ galaxies of our sample have bluer βs than local galaxies at a given extinction level by about –0.4 in β-value. This is in line with ex-

Table 6. Remaining 36 SDF galaxy data

ID	Reduced χ^2	Slope	Metallicity	Age	Escape fraction	E_{B-V}
		β	Z	Myr		mag
(1)	(2)	(3)	(4)	(5)	(6)	(7)
ID02	1.36	−2.41±0.20	0.0068±0.0107	154±183	0.47±0.31	0.0±0.12
ID03	0.29	−2.39±0.17	0.007±0.011	111±129	0.53±0.31	0.2±0.11
ID05	0.20	−2.42±0.20	0.007±0.011	141±171	0.48±0.31	0.0±0.12
ID10	1.05	−2.31±0.20	0.0036±0.0080	407±342	0.44±0.32	0.1±0.12
ID15	0.16	−2.23±0.14	0.0067±0.0082	372±280	0.41±0.32	0.2±0.12
ID20	0.03	−1.80±0.26	0.013±0.016	294±306	0.48±0.32	0.2±0.18
ID21	1.40	−2.17±0.24	0.008±0.012	436±287	0.45±0.32	0.0±0.15
ID22	0.01	−2.14±0.26	0.011±0.016	197±231	0.49±0.31	0.0±0.17
ID23	0.06	−2.26±0.15	0.01±0.01	261±216	0.36±0.29	0.0±0.12
ID24	0.05	−2.31±0.13	0.01±0.01	269±219	0.27±0.24	0.0±0.10
ID25	3.43	−2.11±0.13	0.0056±0.0046	537±134	0.12±0.17	0.1±0.09
ID27	0.52	−2.23±0.23	0.007±0.011	252±222	0.41±0.30	0.2±0.14
ID29	0.02	−2.20±0.25	0.008±0.012	269±224	0.35±0.29	0.0±0.16
ID33	0.0	−2.52±0.14	0.0056±0.0089	142±175	0.22±0.21	0.0±0.08
ID34	0.05	−1.63±0.22	0.008±0.011	294±216	0.44±0.32	0.5±0.15
ID36	0.67	−2.10±0.22	0.010±0.013	248±213	0.49±0.31	0.0±0.16
ID37	0.03	−2.22±0.27	0.012±0.017	125±154	0.52±0.31	0.0±0.16
ID40	1.78	−2.34±0.25	0.006±0.011	160±177	0.48±0.31	0.0±0.15
ID44	0.29	−1.66±0.20	0.009±0.011	271±223	0.36±0.30	0.5±0.15
ID47	0.45	−1.54±0.21	0.012±0.015	180±185	0.48±0.31	0.7±15
ID49	0.02	−1.75±0.32	0.011±0.15	243±213	0.46±0.32	0.4±0.19
ID50	1.52	−1.18±0.23	0.010±0.13	492±152	0.44±0.32	0.6±0.11
ID54	0.50	−2.06±0.27	0.011±0.017	244±215	0.47±0.31	0.0±0.18
ID58	0.19	−1.92±0.27	0.011±0.017	163±188	0.49±0.32	0.5±0.19
ID62	1.21	−2.24±0.19	0.012±0.016	277±202	0.51±0.31	0.0±0.14
ID67	1.10	−1.00±0.20	0.008±0.009	112±166	0.23±0.26	0.4±0.13
ID04	4.97	−2.48±0.20	0.0036±0.0050	332±299	0.48±0.32	0.0±0.08
ID17	5.05	−1.96±0.35	0.0087±0.0126	411±286	0.44±0.32	0.0±0.20
ID31	4.54	−2.69±0.06	0.0011±0.0019	20±53	0.05±0.08	0.0±0.022
ID35	5.15	−1.20±0.15	0.007±0.009	505±123	0.39±0.31	0.5±0.08
ID39	0.0	−2.16±0.29	0.014±0.018	102±131	0.53±0.31	0.25±0.16
ID45	0.25	−1.89±0.35	0.011±0.015	211±206	0.47±0.32	0.2±0.20
ID46	0.0	−2.22±0.30	0.013±0.017	136±164	0.46±0.31	0.1±0.19
ID48	0.0	−1.75±0.35	0.013±0.016	220±208	0.47±0.32	0.1±0.20
ID52	0.11	−1.63±0.33	0.011±0.015	272±216	0.47±0.32	0.2±0.18
ID66	0.0	−1.82±0.38	0.013±0.017	198±202	0.48±0.32	0.3±0.21

NOTE—The best-fit parameters and Bayesian values with errors for implied f_{esc} and UV slope β for the 36 remaining galaxies. **The last 10 galaxies are again the galaxies with no data below the Balmer break as in Table 1.**

pectations, and observations that these galaxies at $z \simeq 6$ are bluer given their particularly younger stellar populations (*e.g.*, **Bouwens et al. 2014**; **Labbé et al. 2010**). Fig. 5b shows the trend between implied $f_{\rm esc}$ and β, and Fig. 5c shows the trend between implied $f_{\rm esc}$ and $E_{\rm B-V}$. At best slight correlations are seen given the large uncertainties, but are in line with the trends seen in Fig. 4.

4. SED MODELS FOR THE 7 J20 GALAXIES

For the 7 galaxies of J20, the implied escape fraction **ranged from ∼0.1-0.5** for the best-fitting CIGALE models, as shown in Fig. 1. For these objects, the inclusion of new K-band data does not significantly alter the fit parameters, but generally confirms the earlier fits with somewhat better χ^2-values. **While the K-band flux for ID28 seems too low considering the other flux values, the SED model in Fig. 1 shows Hβ and [OIII] emission lines redshifted to $\sim 3.6\mu$m, elevating the IRAC data point relative to the K-band continuum.**

From the strong emission lines of Fig. 1 and parameters in Table 1, it is clear that the **7 galaxies of J20** have rather low escape fractions as implied by the CIGALE models. Notably, our results are not significantly affected by the wavelength coverage of our data. Higher signal-to-noise data over a wide wavelength range will be necessary to improve the fits. The *James Webb Space Telescope (JWST)* is able to provide such unique new data, where the *JWST* NIRCam can complement the *HST* WFC3-IR and *Spitzer*/IRAC filters *and* provide much deeper data.

We compared the β measured from J20 and produced by the SED models with the Anderson-Darling test, which gave a statistic of 2.1 and a p-value of 0.04, suggesting that there is a difference between the implied β from the SED models and measured β from J20. Table 1 and 4 show that the CIGALE βs are generally redder than those of J20. This difference may come from the different methods used. J20 used the actual photometry below the restframe Balmer break to derive the β-values, while we used the CIGALE SED modeling to all the data to infer the βs below the restframe Balmer break (i.e., slope for the data versus slope of the model-fit). The currently large uncertainties in the model parameters as fitted by CIGALE come from a lack of deeper data and photometric data points over a wide wavelength range. One method or the other so can't currently be said to be more accurate. Only *JWST* can provide these data, and so better constrain these values with higher accuracy.

We also consider the correlation between dust attenuation and $f_{\rm esc}$ with the CIGALE models. The implied escape fraction modeling can be skewed by the uncertainty in the $E_{\rm B-V}$ extinction, which is an important factor in the escape fraction calculations (*e.g.*, Smith et al. 2018). Overall, the 7 galaxies are consistent with low $E_{\rm B-V}$ values, as expected for blue high redshift star-forming galaxies. Also, the few relatively high escape fractions ($f_{\rm esc}\simeq$0.3–0.4) implied by the CIGALE models are consistent with low dust content, however unusual these may be.

Smith et al. (2020) concluded that for galaxies around $z \simeq 2.3 - 3.5$, the Lyman Continuum is dominated by galaxies with weak AGN, while galaxies without AGN generally have a much lower escape fraction of $f_{\rm esc}\simeq$0.0–0.2, with a rather high uncertainty that comes from the low image signal and the uncertain IGM transmission. The CIGALE SED models for the SDF galaxies studied in this paper suggest low to moderate escape fractions ($f_{\rm esc}\simeq$0–0.6 with a median of ∼0.4) for star-forming galaxies at $z \simeq 6$, but now using a model-dependent indirect method. The trend of escape fraction with redshift in galaxies at $z \simeq 2.3 - 3.5$ seen by Smith et al. (2018, 2020) may thus continue at higher redshifts. Since weak AGN seem to make a substantial contribution to the escaping LyC radiation at $z \simeq 2.3 - 3.5$ (Smith et al. 2020), this may imply that weak AGN are, in general, not present in these 7 SDF galaxies at $z \simeq 6$, in agreement with the modeling of J20. The high implied escape fraction of ID07 could suggest a presence of a weak AGN in this object, although a weak AGN was not obvious from its available Subaru spectra. The completion of reionization at $z \simeq 6$ could have been affected by a higher escape fraction of weak AGN if present at that epoch, although the current SDF data does not require the presence of weak AGN.

The relatively low implied escape fractions for these **7** galaxies may suggest that other factors such as (periodic) outflows in these galaxies caused by supernovae from their young stellar population and/or perhaps from weak AGN, may have created holes in the surrounding ISM of sufficient opening angle to permit **the Lyman Continuum to escape.**

5. SED MODELS FOR THE FULL SAMPLE OF 43 SDF GALAXIES AT $Z \simeq 6$

The full sample of 43 SDF galaxies at $z \simeq 6$ helps constrain which galaxy population(s) could have completed and maintained reionization of the Universe at $z \simeq 6$. **The mean and mode of the escape fraction distri-**

bution of the entire sample is 0.4±0.1 (mean error). Fig. 5b shows that such galaxies have large uncertainties and range in the implied f_{esc} values (∼0.1–0.3). Thus, there may be some overlap between the low and high implied f_{esc} galaxies presented in Fig. 5b. **While the full range of implied f_{esc} values allowed within the fit uncertainties for individual galaxies spans from 0 to ≃ 0.8, the full range does not extend to $f_{esc} = 1.0$. Moreover, the implied values themselves are *all* below $f_{esc} \lesssim 0.6$, and do not scatter to the higher values that would be formally allowed. Thus, the CIGALE models somewhat constrain the range of f_{esc} at $z \simeq 6$.** The median escape fraction value of the 43 SDF galaxies of f_{esc}≃0.4 supports the findings of Finkelstein et al. (2019) and Naidu et al. (2020) that an average escape fraction of at least 10–20% is needed to complete reionization **with UV bright galaxies** by $z \simeq 6$.

Further analysis can be done on the trends between the parameters. The **7 galaxies of J20** have a larger fraction of objects with lower implied f_{esc} values, while most of the remaining 36 SDF galaxies do generally have larger implied f_{esc} values. **The Anderson-Darling test between the two samples gives a statistic of 3.03 with a significance of 0.02**, so the two distributions seem to differ. **The 7 galaxies were chosen to have blue slopes in J20, so to test how galaxies with bluer β-values might differ from redder galaxies, Fig. 4 shows cumulative distributions and Gaussians of two subsamples of the 14 galaxies that showed correlation between f_{esc} and their χ^2 value: bluer galaxies ($\beta \lesssim -2.35$) and redder galaxies (β-values $\gtrsim -2.35$). Fig. 4a and b show that the bluer subsample has its distribution peaking around $\beta \simeq -2.6$, while the redder subsample has its distribution peaking around $\beta \simeq -2.2$. Fig. 4c and d show that the bluer subsample has smaller implied E_{B-V} -values with a median $E_{B-V} \simeq 0.1$ mag, while the redder subsample has a higher median near $E_{B-V} \simeq 0.4$ mag. Finally, Fig. 4e and f show that the bluer subsample has smaller implied f_{esc} values, with a mode and median of around f_{esc}≃0.1, while the redder subsample has larger implied f_{esc} values at f_{esc}≃0.3 being the most probable, and a median value at f_{esc}≃0.4–0.45. The Anderson-Darling test between two subsamples' f_{esc} returns a p-value of 0.006, so the samples do differ.**

The trend of f_{esc} increasing slightly with redder β can also be seen in Fig. 5. Fig 5a indicates that bluer implied β corresponds with lower implied E_{B-V} values. At given CIGALE-fit E_{B-V} values, the implied β-values at $z \simeq 6$ seem to be steeper than those at $z \simeq 0$ found from the Calzetti/Meurer relation (Calzetti et al. 2000; Meurer et al. 1999) by about –0.4 in β. This is expected, and agrees with observations (*e.g.*, **Bouwens et al. 2014; Labbé et al. 2010**), since higher redshift galaxies tend to have younger stellar populations and lower metallicity and extinction, and therefore bluer UV-continuum than low redshift galaxies.

Fig. 5b and 5c also suggest that lower implied f_{esc} is associated with bluer β and lower E_{B-V} . The f_{esc}-β correlation suggests that the LyC is absorbed more readily in bluer galaxies and predicts that they will have stronger nebular line emission. The correlation between f_{esc} and E_{B-V} is contrary to that observed in local galaxies, where the f_{esc}-value drops in systems that have more significant dust extinction (Verhamme et al. 2008). **Both trends also appear to differ from results from a spectroscopic study of UV-bright galaxies at $z \sim 3$, where larger E_{B-V} and redder colors appear robustly associated with lower ratios of emergent ionizing to non-ionizing UV flux density (Steidel et al. 2018). This apparent discrepancy motivates a more direct comparison between our results and studies at lower redshifts in order to control for the likely dependence of f_{esc} on UV luminosity and use spectroscopic data to assess our SED-fitting technique, but such a study is beyond the scope of our current effort. If our results are confirmed via future spectroscopic campaigns, then they may indicate significant cosmological evolution in the ISM properties of star-forming galaxies. Likewise, they may support theoretical predictions that f_{esc} could vary with halo mass (Paardekooper et al. 2013, 2015; Ma et al. 2020), perhaps even non-monotonically (Ma et al. 2020), and increase with redshift at fixed halo mass (Alvarez et al. 2012; Paardekooper et al. 2013; Ma et al. 2020). These predictions remain sensitive to uncertain details of numerical and physical treatments (compare, for example, Ma et al. 2015 and Ma et al. 2020), and would therefore benefit from observational guidance.**

We have investigated the possibility that the f_{esc}-β correlation is an artifact emerging from the fact that CIGALE does not distinguish between young galaxies with strong line emission and mature ones with a larger Balmer break. Misidentifying more mature galaxies as younger ones could overestimate the line fluxes from the contribution of the Balmer break, inflating f_{esc}. To test if this problem truly existed, a single galaxy

was modeled multiple times, but each with flux values slightly shifted with random values within uncertainty. If CIGALE did not distinguish the two sets of galaxies, lower f_{esc} should always have yielded steeper β-values. However, this was not always the case, as some models with lower f_{esc} had higher β than models with higher f_{esc}. In conclusion, there thus seem to be mild correlations at $z \simeq 6$ between the CIGALE model f_{esc}, β, and E_{B-V} -values, in the sense that the implied f_{esc} may trend to higher values for both redder model β and for higher model E_{B-V} values.

These trends, if real and supported by *JWST* data, may suggest that galaxies with higher star-formation rates may have produced more dust and extinction with higher E_{B-V} and somewhat redder β, as their stellar population may have needed to age enough (*i.e.*, ages $\gtrsim$ 3–30 Myr) for supernovae to have occurred, additional dust to be created (*e.g.*, **Dayal 2019**), and β to have further flattened and reddened**; indeed, similar correlations are well-documented at $z \sim$2–3.5 (for example Papovich et al. 2001; Pilo et al. 2019).** The somewhat higher implied f_{esc} values may then require the somewhat older and redder stellar populations with more dust to have created sufficient holes in the ISM (due to, *e.g.*, SNe and/or weak AGN outflows), so that LyC can escape at least for a period of time, which may be related to the age of their immediate past stellar population**; this is in fact predicted at $z > 5$ for galaxies forming in halos with masses of 10^8–$10^{9.5} M_\odot$ (Ma et al. 2020).**

Our results confirm previous observations that a range of f_{esc}may be expected for any β or E_{B-V} value (Shapley et al. 2006). Cosmological simulations predict such large variations (Paardekooper et al. 2015; Smith et al. 2019), attributing them to differences in the geometry and porosity of galaxies' ISM (see also Smith et al. 2018) and circumgalactic media that may allow certain lines-of-sight *into the galaxy* to provide higher LyC escape fractions than others (Ma et al. 2020). In addition to a dependence of f_{esc} on orientation, simulations predict that f_{esc} fluctuates rapidly, with short-lived spikes in LyC luminosity following brief star-formation episodes (Smith et al. 2019). The large resulting scatter in f_{esc} can only be characterized through reference to large galaxy samples, as we have attempted to do. Our CIGALE modeling suggests an overall escape fraction of $f_{esc} \sim 0.4$, which exceeds some theoretical predictions (for example, Paardekooper et al. 2015; Ma et al. 2020) although it matches (and may even exceed) requirements for galaxies to complete and maintain the cosmological hydrogen reionization by $z \simeq 6$ (for example, Finkelstein et al. 2019).

6. SUMMARY

We extended the sample of $z \simeq 6$ Lyα emitting galaxies within the Subaru Deep Field with detailed SED analyses from 7 Jiang et al. (2013) to 43. Each of these galaxies had extant ground- and space-based optical–IR observations of sufficient quality and depth to constrain their SEDs. All SED fitting, starting with the 7 galaxies modeled in J20, was performed here using the CIGALE package (Boquien et al. 2019). Using the best-fitting CIGALE models, we investigated trends between physical parameters, such as the fitted UV slope, β, the fitted extinction, E_{B-V} , and the implied escape fractions, f_{esc}, to infer what factors may have affected reionization at $z \simeq 6$.

From the models of the 7 galaxies of J20, we suggested that there may be a mild correlation between lower escape fraction with steeper βs. The implied ages of the galaxies ranged from **10 to 800** Myr, and the implied metallicity from 0.0001 to 0.05, indicating that a wide range of parameter values is possible for galaxies with blue β at $z \simeq 6$.

We obtained similar conclusions — but with better statistics — for the full sample of 43 galaxies at $z \simeq 6$. We found that galaxies at $z \simeq 6$ may have an *median escape fraction as implied by CIGALE* of $f_{esc} \simeq$**0.4±0.1 (mean error). While the current uncertainties remain large, this f_{esc}-values implied by CIGALE do not span the entire f_{esc} range, and could be improved with deeper observations over a wider wavelength range to improve the SED models. Furthermore, when considering only the galaxies that showed correlation between their model fits and f_{esc} and the full sample, a possible correlation between bluer β and lower implied f_{esc} was found.** It is notable that implied β were steeper at given model E_{B-V} values for $z \simeq 6$ galaxies, when compared to galaxies at $z \simeq 0$ as found by Calzetti et al. (*e.g.*, 2000) and Meurer et al. (1999). If these trends are confirmed with higher signal-to-noise ratio *JWST* data, this may suggest that LyC could have escaped through holes in the ISM from the SNe or AGN in somewhat older stellar populations.

The correlations found between the parameters are still weak given the significant uncertainties in the data and the modeling. To better constrain the CIGALE models, more accurate data and spectroscopic observations further into the infrared range will

be needed. Currently, only shallow *Spitzer* and Hershel data are available. Furthermore, the spectra of the galaxies, from which their redshift were derived, does not cover a wide-enough wavelength range to provide additional constraints to the available broadband data for better SED fitting. Future deeper spectral observations, such as with *JWST* NIRSpec at 1–5 μm, would provide much better constraints to their SED parameters. At $z \simeq 6$, the *JWST/NIRSpec* will be able to observe Hβ and [OIII] emission lines at 3.0–3.5 μm, which will provide much better constraints on the CIGALE models than using broadband fluxes alone. The newly included K-band data supported the accuracy of the **7** galaxy models of J20 and improved at least one model, which demonstrated the need for additional 1.6–5 μm data points with *JWST* to confirm these results.

Another way to approach this problem will be to use the available spectra to estimate the physical parameters of these galaxies at $z \simeq 6$. The quality of the spectra will have to be high to make such estimates possible, and to make a better comparison between the CIGALE models and the available data. With higher accuracy data and spectroscopy further into the infrared, the characteristics of galaxies with steep β and the escape fractions of high redshift galaxies can be better characterized to more fully constrain the sources of the reionization of the Universe at $z \simeq 6$.

ACKNOWLEDGMENTS

We thank the anonymous referee; their report helped us clarify and significantly improve our manuscript, and pointed us to the Anderson-Darling test. We also thank Ian Smail and Pratika Dayal for discussions and several relevant references. Based on observations made with the NASA/ESA Hubble Space Telescope, obtained at the Space Telescope Science Institute. Support for HST program GO15137 was provided by NASA through a grant from the Space Telescope Science Institute, which is operated by the Association of Universities for Research in Astronomy, Inc., under NASA contract NAS 5-26555. RAW acknowledges support from NASA *JWST* Interdisciplinary Scientist grants NAG5-12460, NNX14AN10G and 80NSSC18K0200 from GSFC.

Facilities: *HST*(ACS, WFC3/UVIS, WFC3/IR), Subaru(HSC), *Spitzer*/IRAC, UKIRT/WFCAM

Software: astropy (Astropy Collaboration et al. 2018), CIGALE (Boquien et al. 2019)

REFERENCES

Alvarez, M. A., Finlator, K., & Trenti, M. 2012, ApJL, 759, L38, doi: 10.1088/2041-8205/759/2/L38

Astropy Collaboration, Price-Whelan, A. M., SipHocz, B. M., et al. 2018, aj, 156, 123, doi: 10.3847/1538-3881/aabc4f

Barrow, K. S. S., Robertson, B. E., Ellis, R. S., et al. 2020, ApJL, 902, L39, doi: 10.3847/2041-8213/abbd8e

Bertin, E., & Arnouts, S. 1996, A&AS, 117, 393, doi: 10.1051/aas:1996164

Boquien, M., Burgarella, D., Roehlly, Y., et al. 2019, A&A, 622, A103, doi: 10.1051/0004-6361/201834156

Bouwens, R. J., Illingworth, G. D., Oesch, P. A., et al. 2014, ApJ, 793, 115, doi: 10.1088/0004-637X/793/2/115

Calzetti, D., Armus, L., Bohlin, R. C., et al. 2000, ApJ, 533, 682, doi: 10.1086/308692

Dayal, P. 2019, Proceedings of the International Astronomical Union, 15, 43–43, doi: 10.1017/s1743921320001106

Finkelstein, S. L., D'Aloisio, A., Paardekooper, J.-P., et al. 2019, ApJ, 879, 36, doi: 10.3847/1538-4357/ab1ea8

Furusawa, H., Kosugi, G., Akiyama, M., et al. 2008, ApJS, 176, 1, doi: 10.1086/527321

Gardner, J. P., Mather, J. C., Clampin, M., et al. 2006, SSRv, 123, 485, doi: 10.1007/s11214-006-8315-7

Grogin, N. A., Kocevski, D. D., Faber, S. M., et al. 2011, ApJS, 197, 35, doi: 10.1088/0067-0049/197/2/35

Hayes, M., Schaerer, D., Östlin, G., et al. 2011, ApJ, 730, 8, doi: 10.1088/0004-637X/730/1/8

Hewett, P. C., Warren, S. J., Leggett, S. K., & Hodgkin, S. T. 2006, MNRAS, 367, 454, doi: 10.1111/j.1365-2966.2005.09969.x

Hodgkin, S. T., Irwin, M. J., Hewett, P. C., & Warren, S. J. 2009, MNRAS, 394, 675, doi: 10.1111/j.1365-2966.2008.14387.x

Jiang, L., Cohen, S. H., Windhorst, R. A., et al. 2020, ApJ, 889, 90, doi: 10.3847/1538-4357/ab64ea

Jiang, L., Egami, E., Mechtley, M., et al. 2013, ApJ, 772, 99, doi: 10.1088/0004-637X/772/2/99

Jiang, L., Finlator, K., Cohen, S. H., et al. 2016, ApJ, 816, 16, doi: 10.3847/0004-637X/816/1/16

Joye, W. A., & Mandel, E. 2003, in Astronomical Society of the Pacific Conference Series, Vol. 295, Astronomical Data Analysis Software and Systems XII, ed. H. E. Payne, R. I. Jedrzejewski, & R. N. Hook, 489

Kashikawa, N., Shimasaku, K., Matsuda, Y., et al. 2011, ApJ, 734, 119, doi: 10.1088/0004-637X/734/2/119

Keating, L. C., Kulkarni, G., Haehnelt, M. G., Chardin, J., & Aubert, D. 2020, MNRAS, 497, 906, doi: 10.1093/mnras/staa1909

Kim, D., Jansen, R. A., & Windhorst, R. A. 2017, ApJ, 840, 28, doi: 10.3847/1538-4357/aa6ba1

Koekemoer, A. M., Faber, S. M., Ferguson, H. C., et al. 2011, ApJS, 197, 36, doi: 10.1088/0067-0049/197/2/36

Kotulla, R., Fritze, U., Weilbacher, P., & Anders, P. 2009, MNRAS, 396, 462, doi: 10.1111/j.1365-2966.2009.14717.x

Labbé, I., González, V., Bouwens, R. J., et al. 2010, ApJL, 716, L103, doi: 10.1088/2041-8205/716/2/L103

Lawrence, A., Warren, S. J., Almaini, O., et al. 2007, MNRAS, 379, 1599, doi: 10.1111/j.1365-2966.2007.12040.x

Loeb, A., & Barkana, R. 2001, ARA&A, 39, 19, doi: 10.1146/annurev.astro.39.1.19

Ma, X., Kasen, D., Hopkins, P. F., et al. 2015, MNRAS, 453, 960, doi: 10.1093/mnras/stv1679

Ma, X., Quataert, E., Wetzel, A., et al. 2020, MNRAS, 498, 2001, doi: 10.1093/mnras/staa2404

Maseda, M. V., Franx, M., Chevallard, J., & Curtis-Lake, E. 2019, MNRAS, 486, 3290, doi: 10.1093/mnras/stz818

McLure, R. J., Dunlop, J. S., de Ravel, L., et al. 2011, MNRAS, 418, 2074, doi: 10.1111/j.1365-2966.2011.19626.x

Meurer, G. R., Heckman, T. M., & Calzetti, D. 1999, ApJ, 521, 64, doi: 10.1086/307523

Miralda-Escudé, J., Haehnelt, M., & Rees, M. J. 2000, ApJ, 530, 1, doi: 10.1086/308330

Naidu, R. P., Tacchella, S., Mason, C. A., et al. 2020, ApJ, 892, 109, doi: 10.3847/1538-4357/ab7cc9

Noll, S., Burgarella, D., Giovannoli, E., et al. 2009, A&A, 507, 1793, doi: 10.1051/0004-6361/200912497

Oesch, P. A., Labbé, I., Bouwens, R. J., et al. 2013, ApJ, 772, 136, doi: 10.1088/0004-637X/772/2/136

Oke, J. B., & Gunn, J. E. 1983, ApJ, 266, 713, doi: 10.1086/160817

Ono, Y., Ouchi, M., Shimasaku, K., et al. 2010, ApJ, 724, 1524, doi: 10.1088/0004-637X/724/2/1524

Paardekooper, J. P., Khochfar, S., & Dalla, C. V. 2013, MNRAS, 429, L94, doi: 10.1093/mnrasl/sls032

Paardekooper, J.-P., Khochfar, S., & Dalla Vecchia, C. 2015, MNRAS, 451, 2544, doi: 10.1093/mnras/stv1114

Papovich, C., Dickinson, M., & Ferguson, H. C. 2001, ApJ, 559, 620, doi: 10.1086/322412

Pilo, S., Castellano, M., Fontana, A., et al. 2019, A&A, 626, A45, doi: 10.1051/0004-6361/201834442

Ryan, R. E. 2011, iGalFit: An Interactive Tool for GalFit. https://arxiv.org/abs/1110.1090

Schaerer, D., & de Barros, S. 2009, A&A, 502, 423, doi: 10.1051/0004-6361/200911781

Shapley, A. E., Steidel, C. C., Adelberger, K. L., et al. 2001, ApJ, 562, 95, doi: 10.1086/323432

Shapley, A. E., Steidel, C. C., Erb, D. K., et al. 2005, ApJ, 626, 698, doi: 10.1086/429990

Shapley, A. E., Steidel, C. C., Pettini, M., Adelberger, K. L., & Erb, D. K. 2006, ApJ, 651, 688, doi: 10.1086/507511

Smith, A., Ma, X., Bromm, V., et al. 2019, MNRAS, 484, 39, doi: 10.1093/mnras/sty3483

Smith, B. M., Windhorst, R. A., Jansen, R. A., et al. 2018, ApJ, 853, 191, doi: 10.3847/1538-4357/aaa3dc

Smith, B. M., Windhorst, R. A., Cohen, S. H., et al. 2020, ApJ, 897, 41, doi: 10.3847/1538-4357/ab8811

Steidel, C. C., Bogosavljević, M., Shapley, A. E., et al. 2018, ApJ, 869, 123, doi: 10.3847/1538-4357/aaed28

Trenti, M., Bradley, L. D., Stiavelli, M., et al. 2011, ApJL, 727, L39, doi: 10.1088/2041-8205/727/2/L39

Verhamme, A., Schaerer, D., Atek, H., & Tapken, C. 2008, A&A, 491, 89, doi: 10.1051/0004-6361:200809648

Windhorst, R. A., Timmes, F. X., Wyithe, J. S. B., et al. 2018, ApJS, 234, 41, doi: 10.3847/1538-4365/aaa760

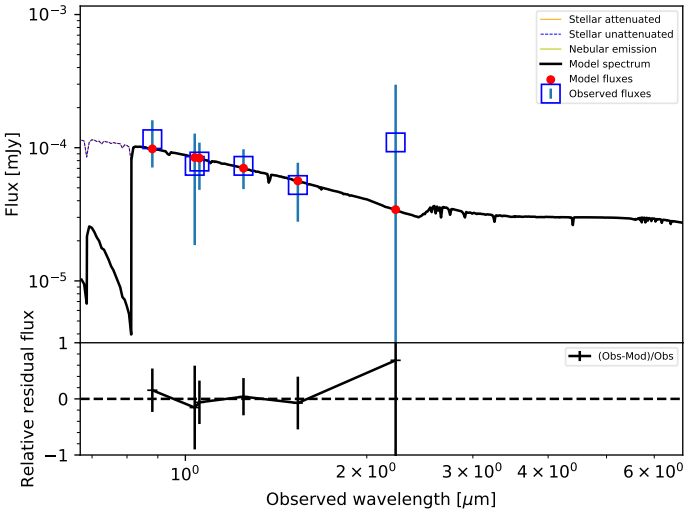

(ID07)

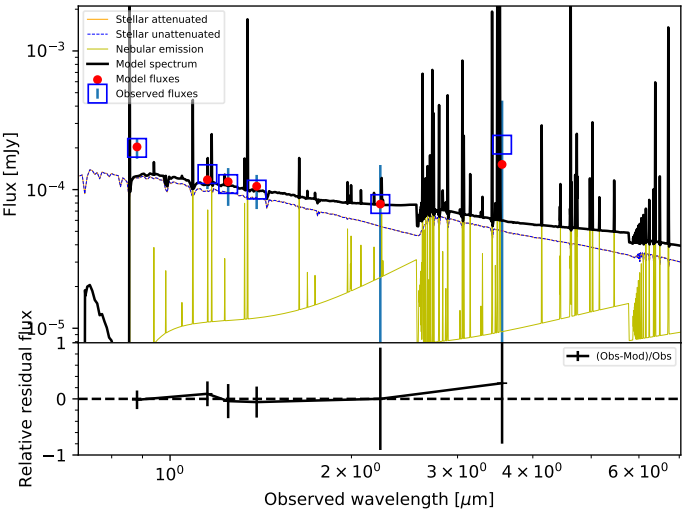

(ID28)

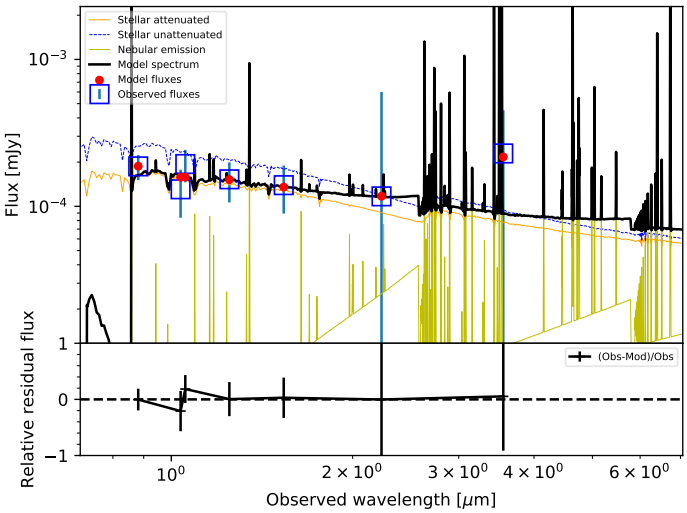

(ID30)

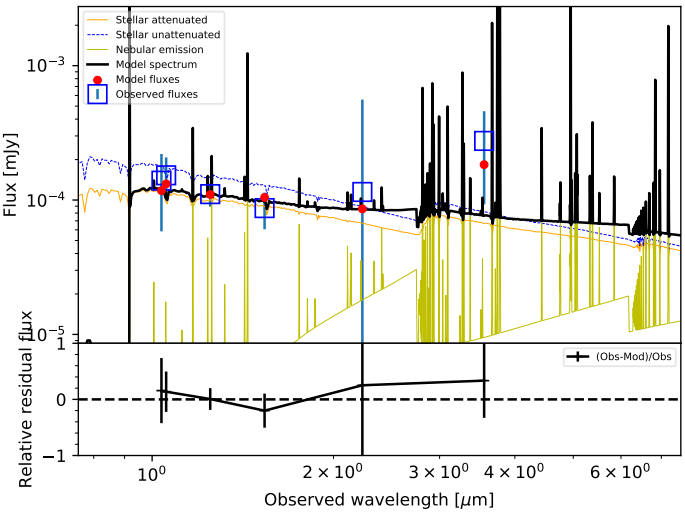

(ID43)

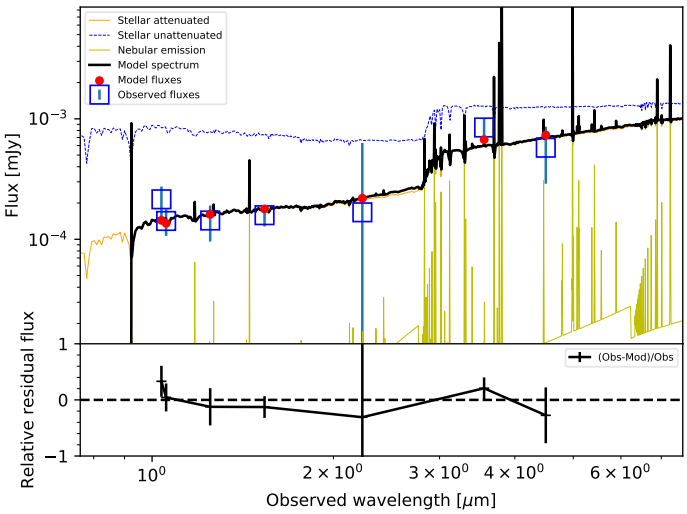

(ID61)

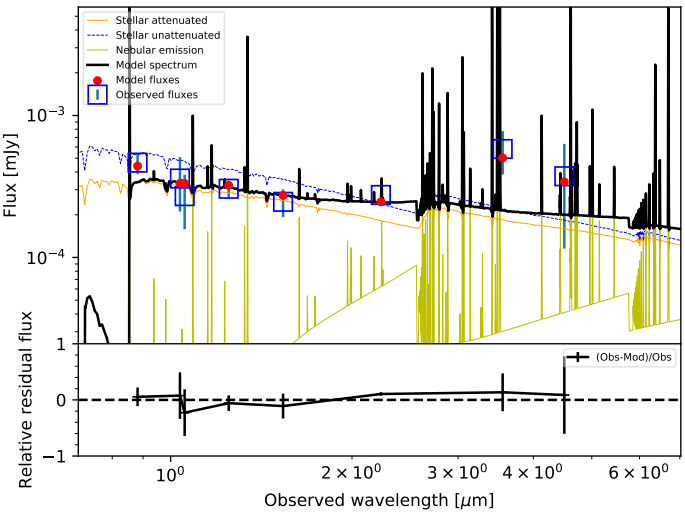

(ID63)

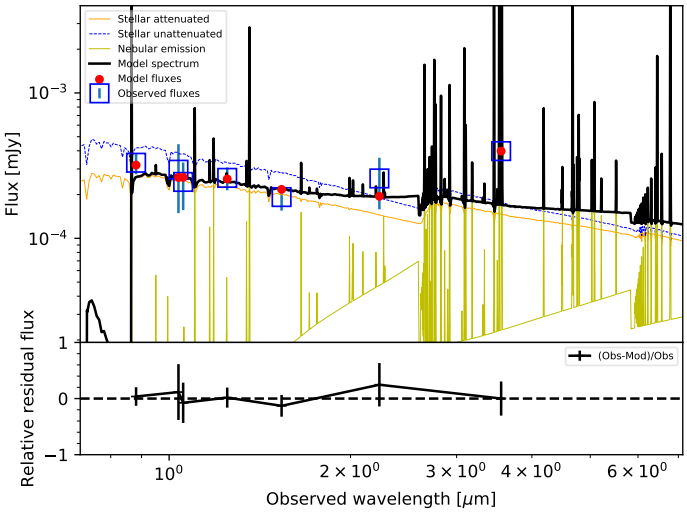

(ID64)

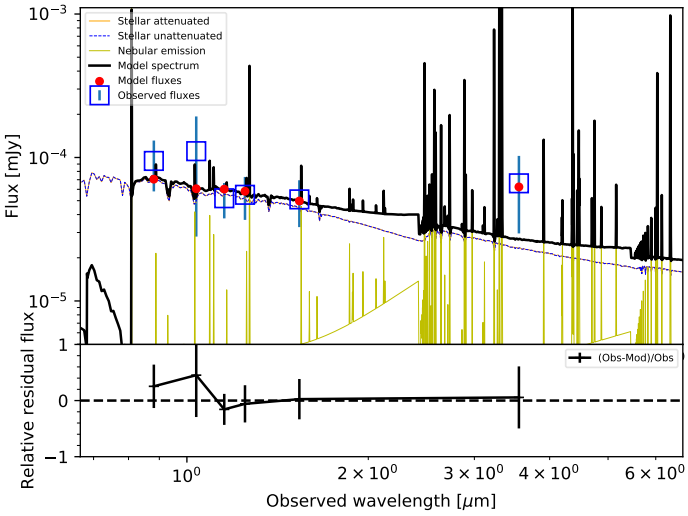

(ID02)

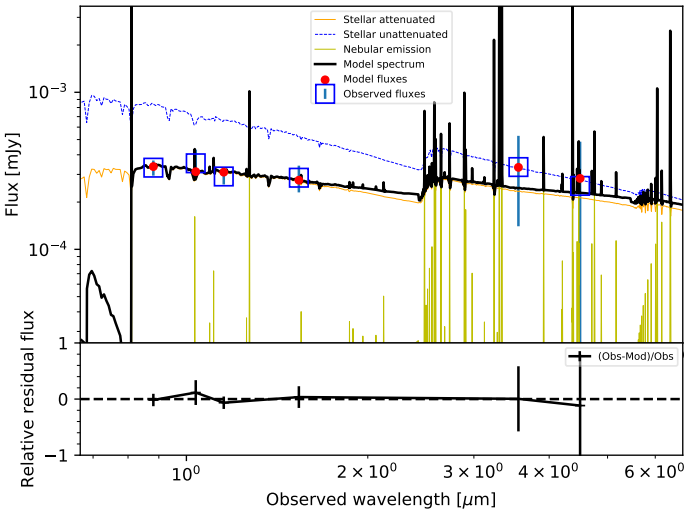

(ID03)

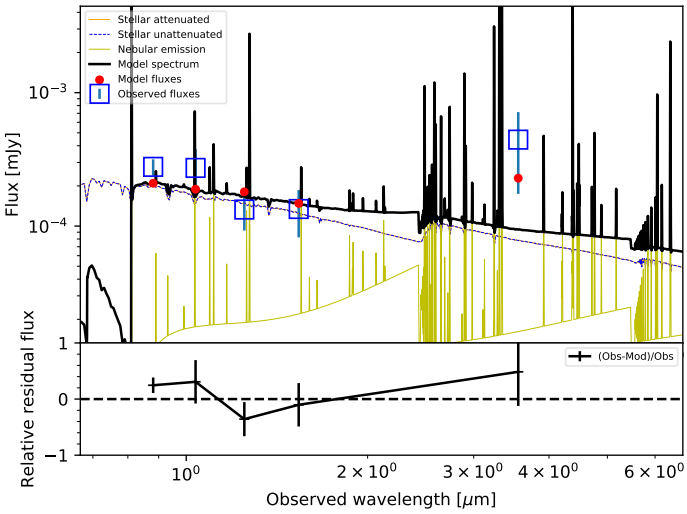

(ID04)

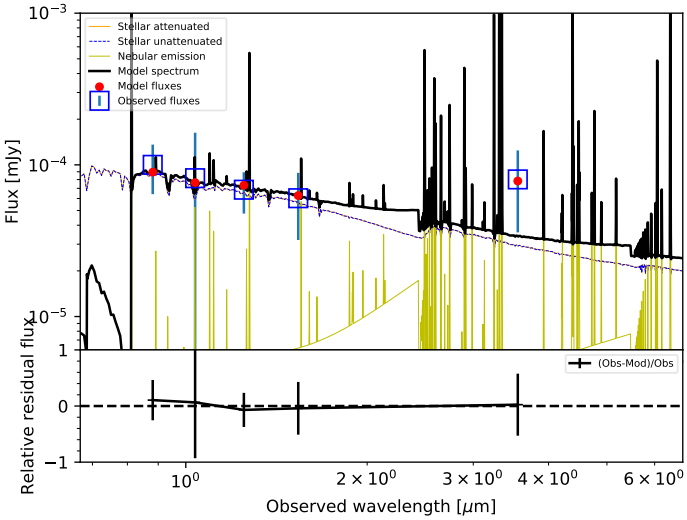

(ID05)

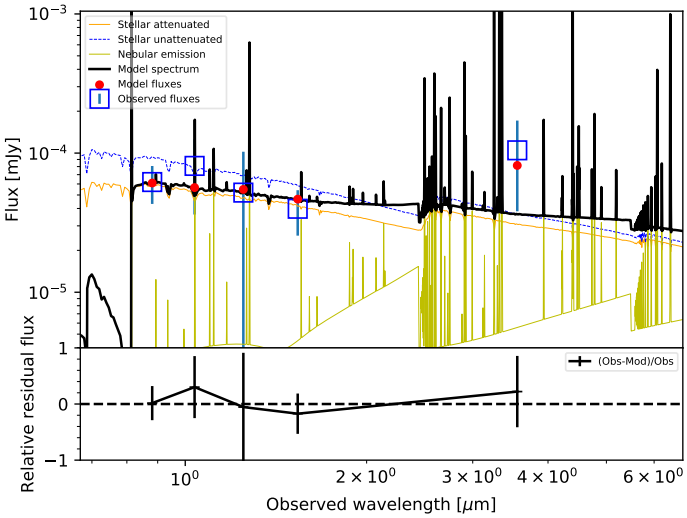

(ID10)

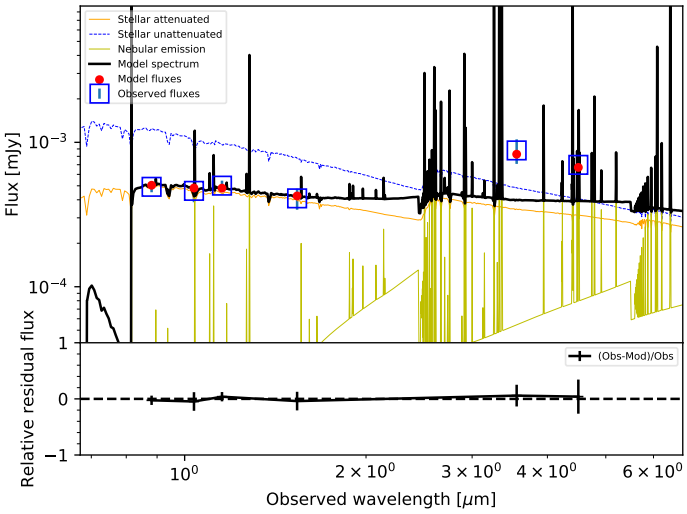

(ID15)

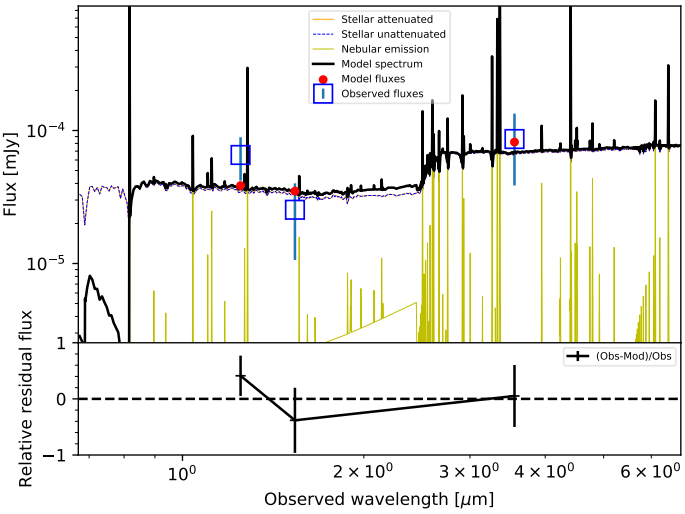

(ID17)

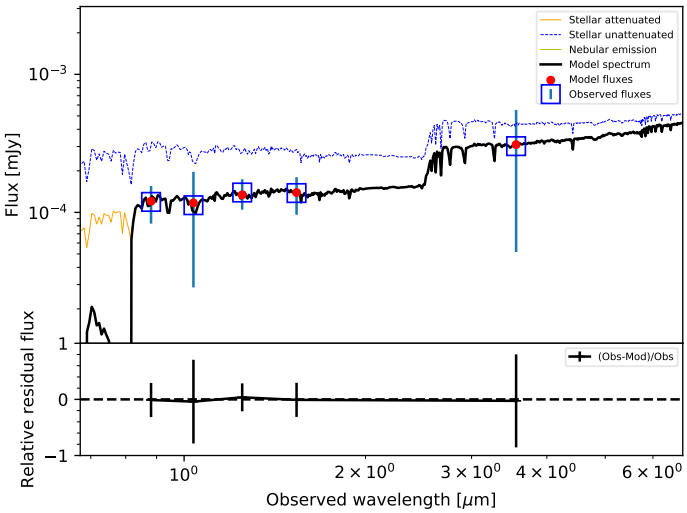

(ID20)

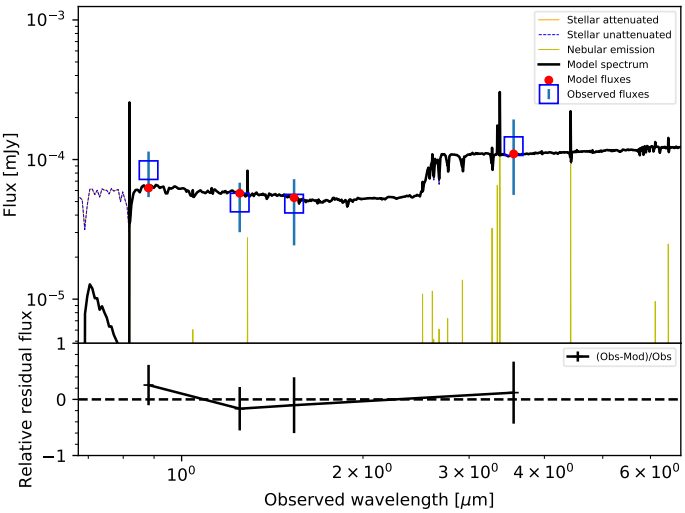

(ID21)

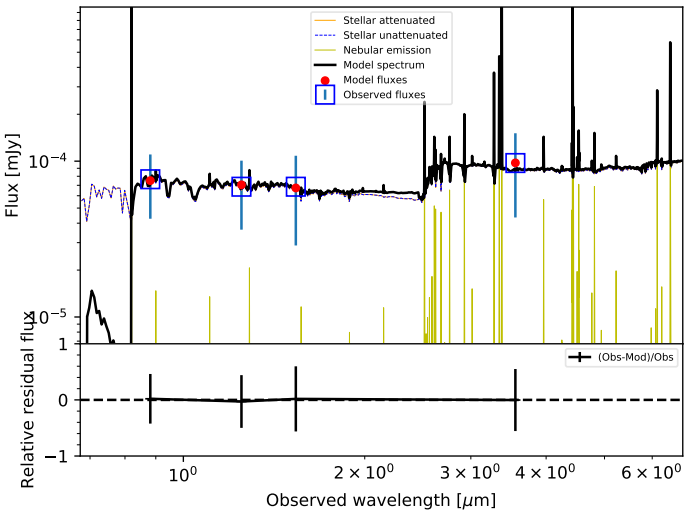

(ID22)

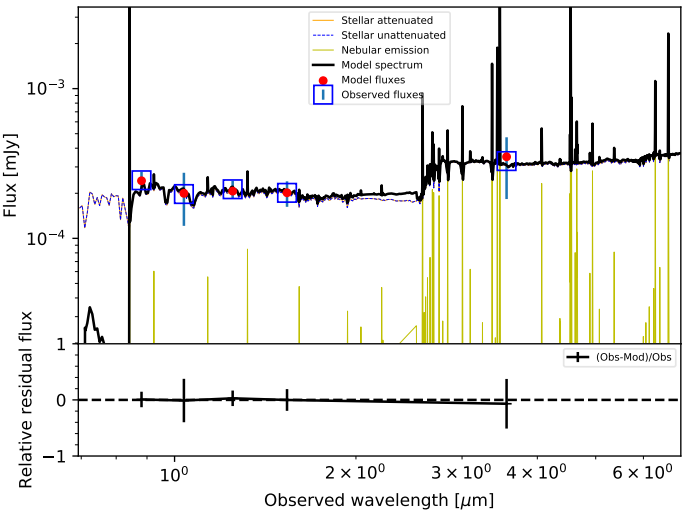

(ID23)

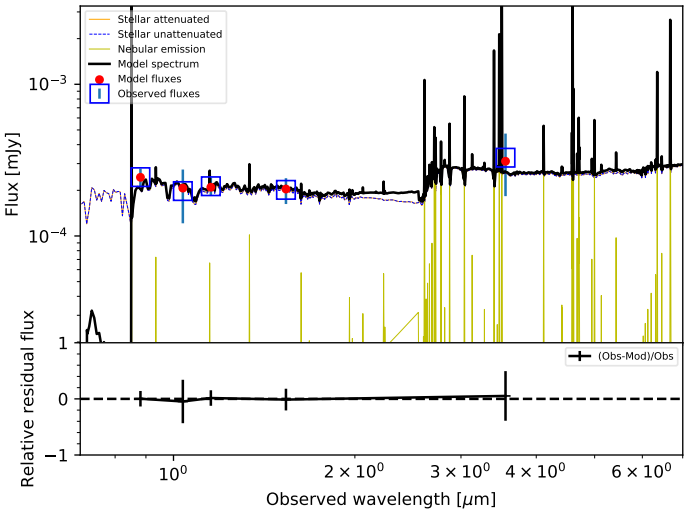

(ID24)

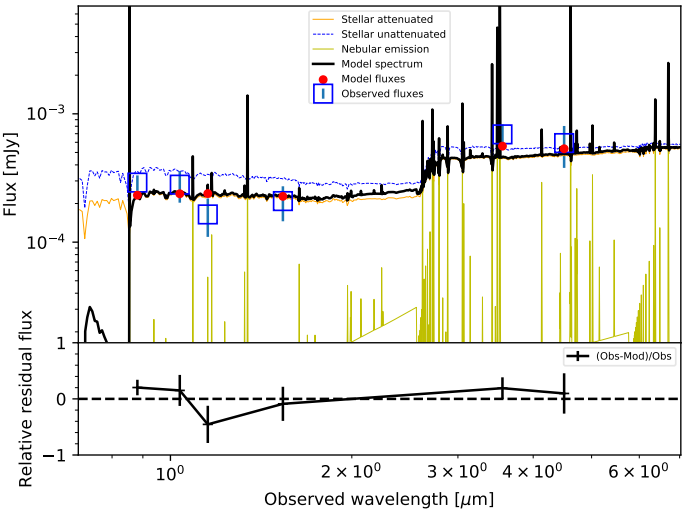

(ID25)

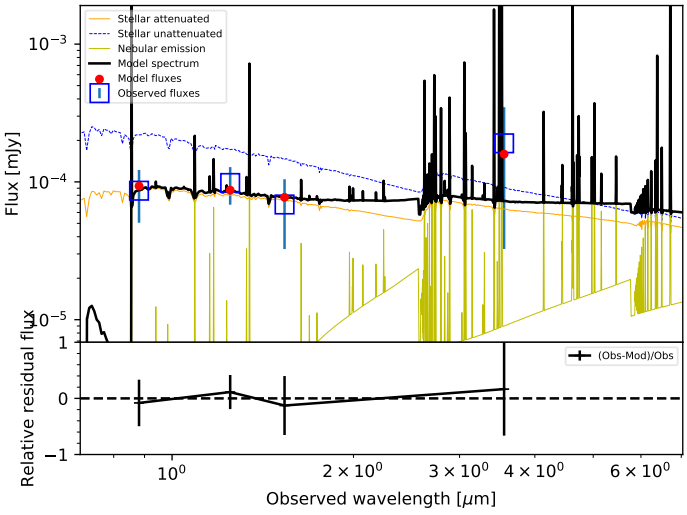

(ID27)

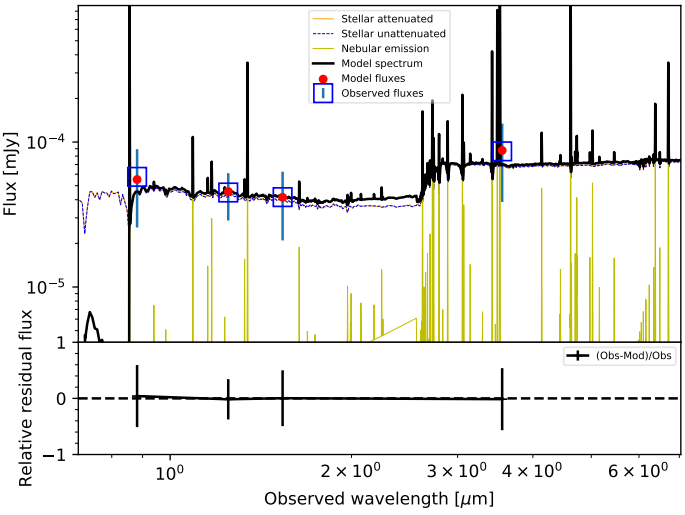

(ID29)

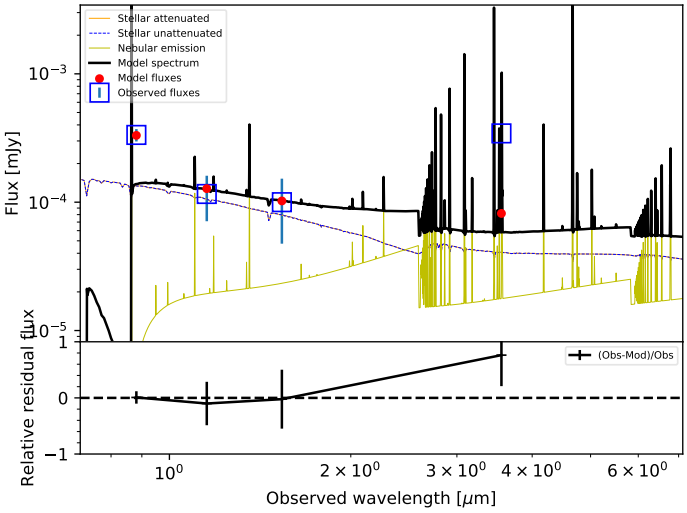

(ID31)

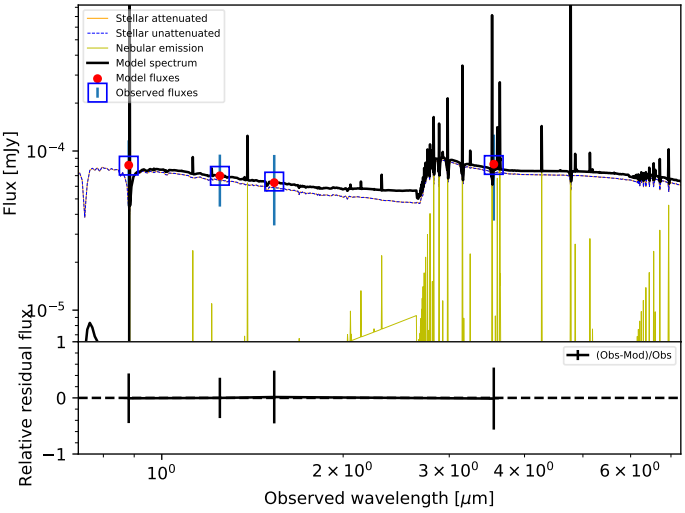

(ID33)

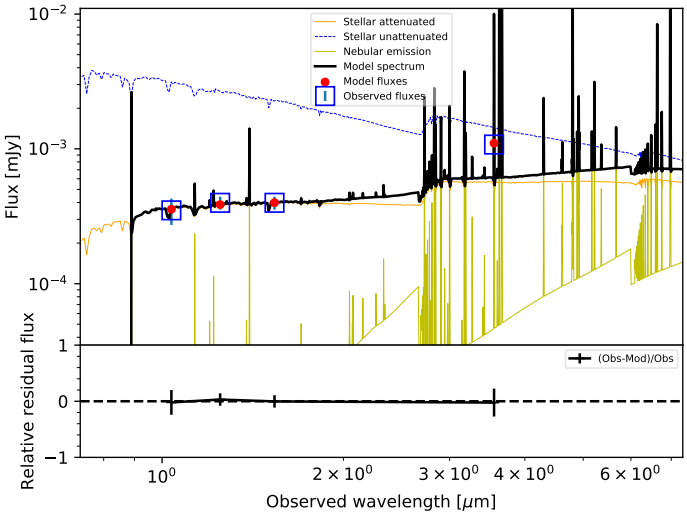

(ID34)

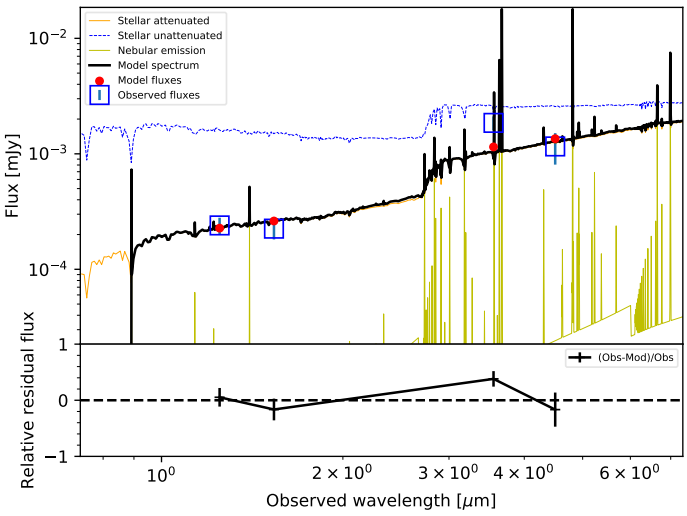

(ID35)

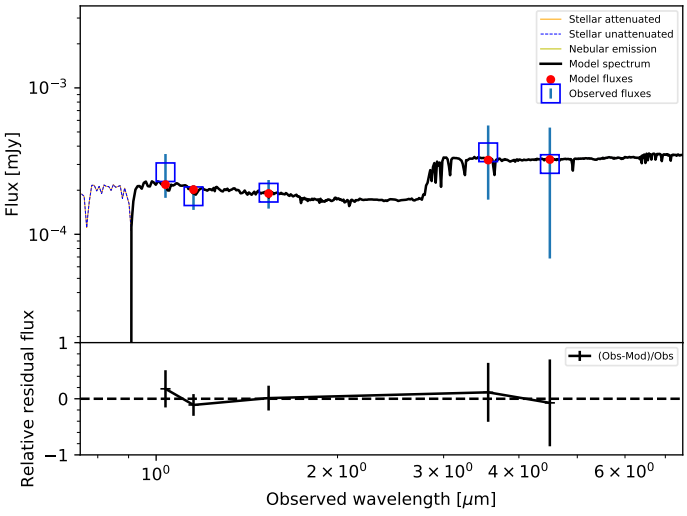

(ID36)

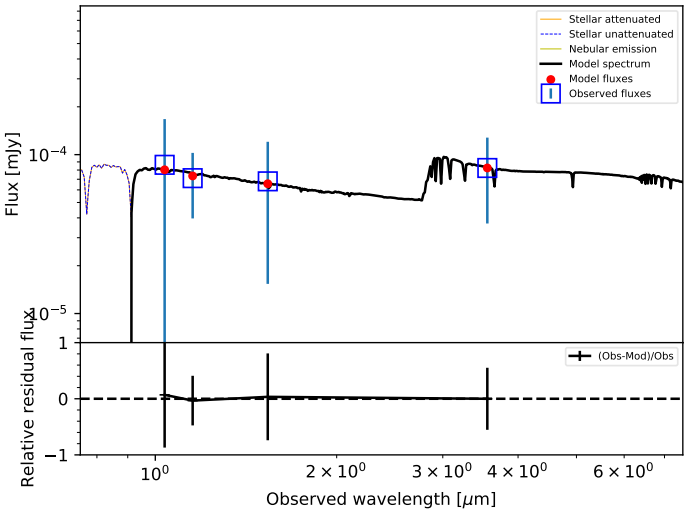

(ID37)

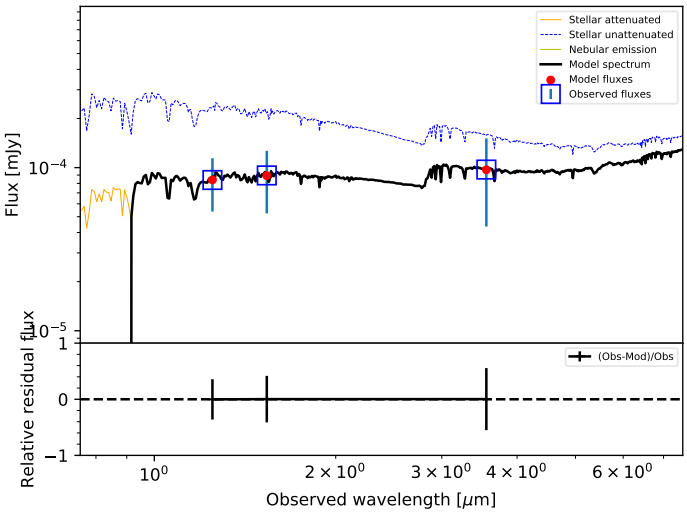

(ID39)

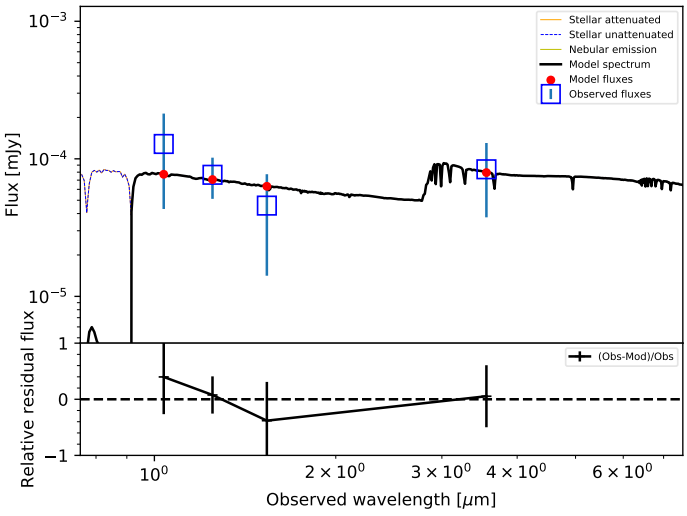

(ID40)

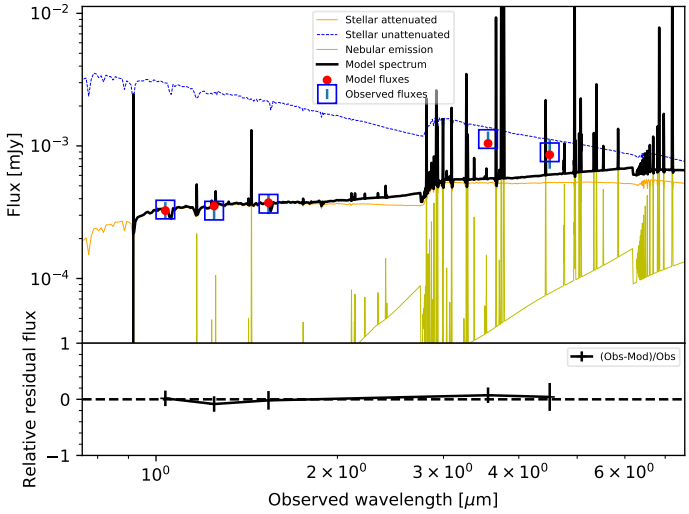

(ID44)

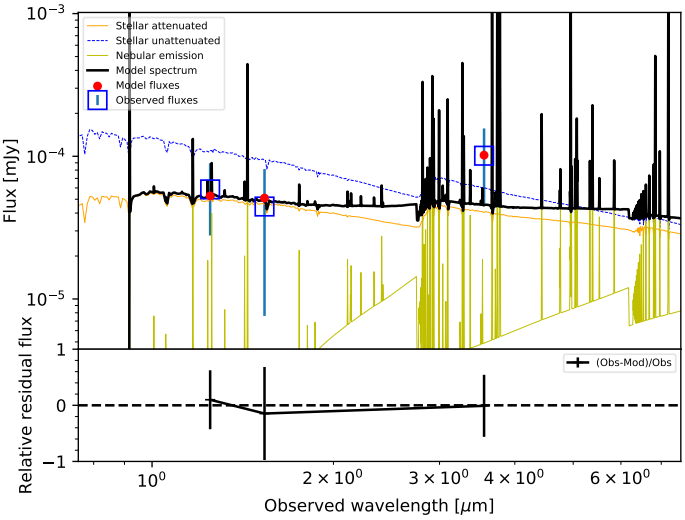

(ID45)

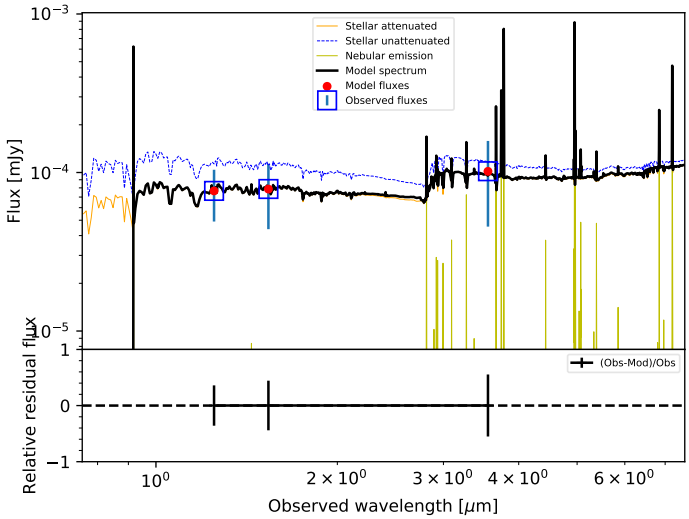

(ID46)

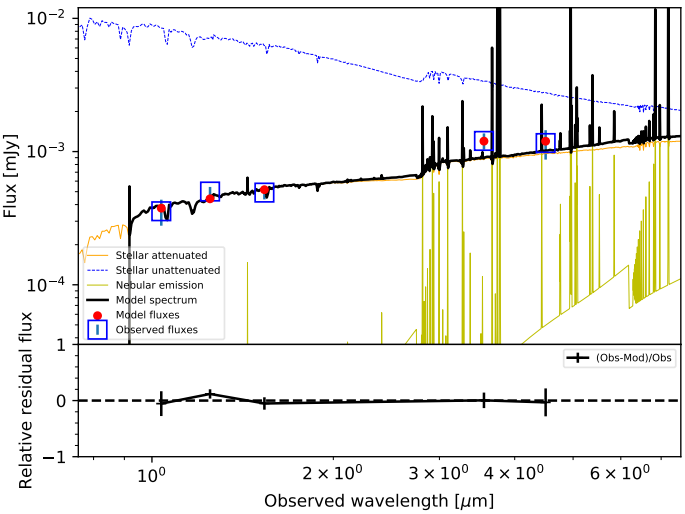

(ID47)

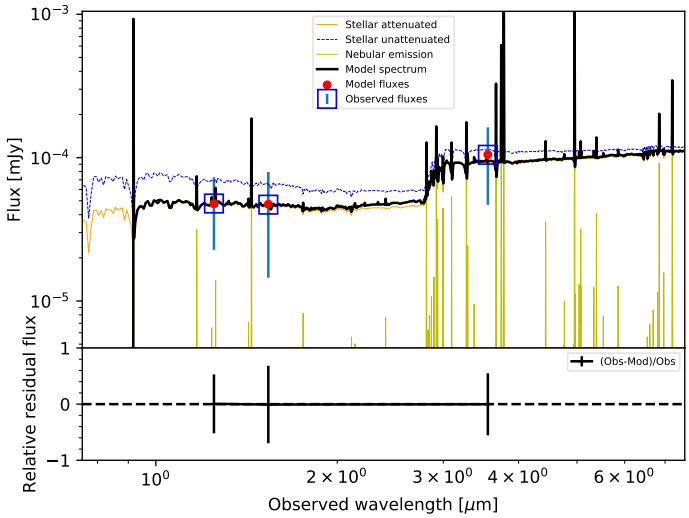

(ID48)

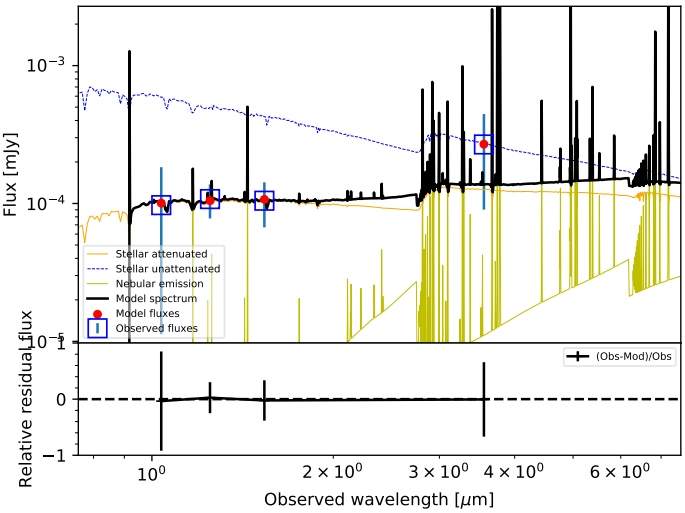

(ID49)

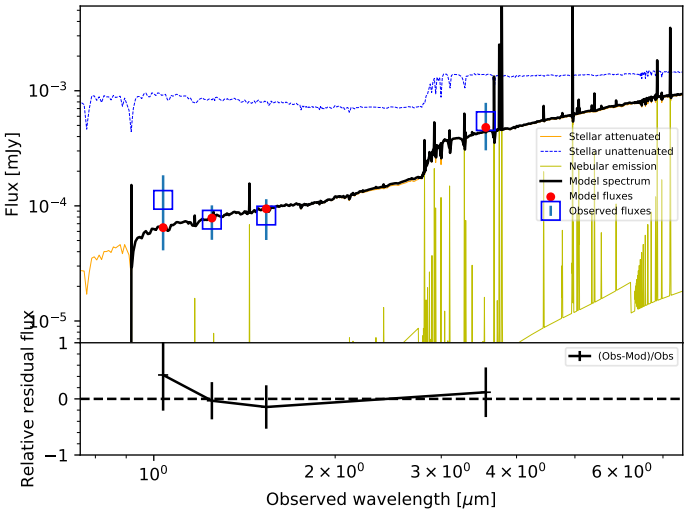

(ID50)

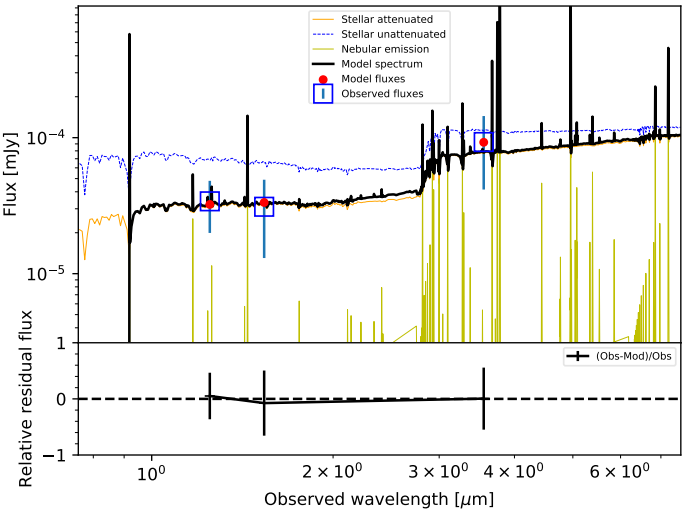

(ID52)

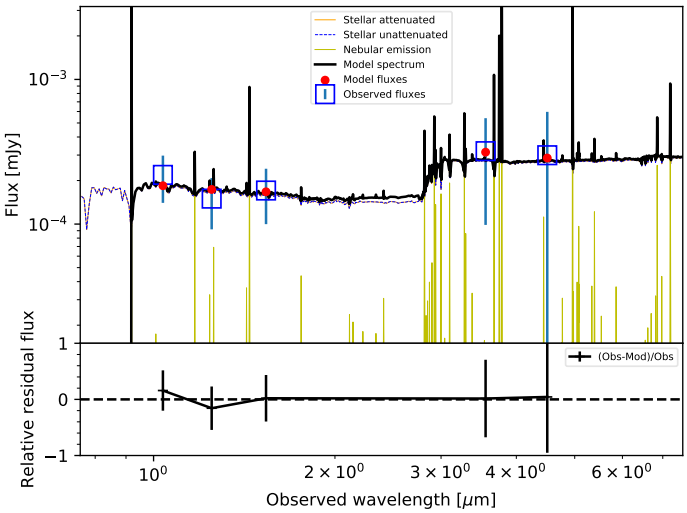

(ID54)

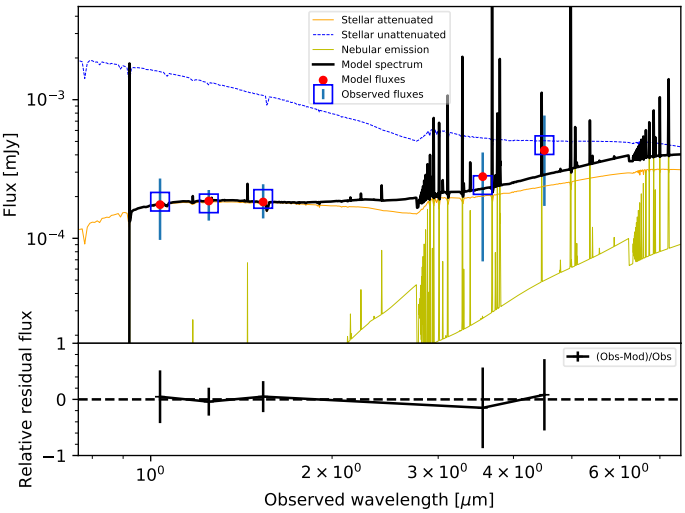

(ID58)

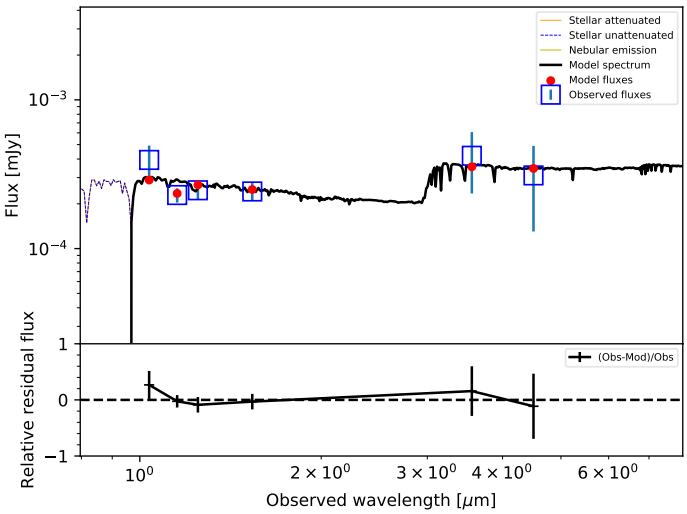

(ID62)

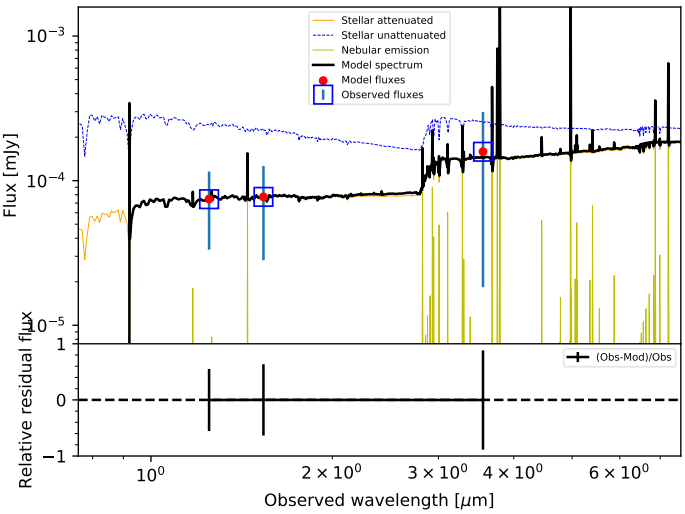

(ID66)

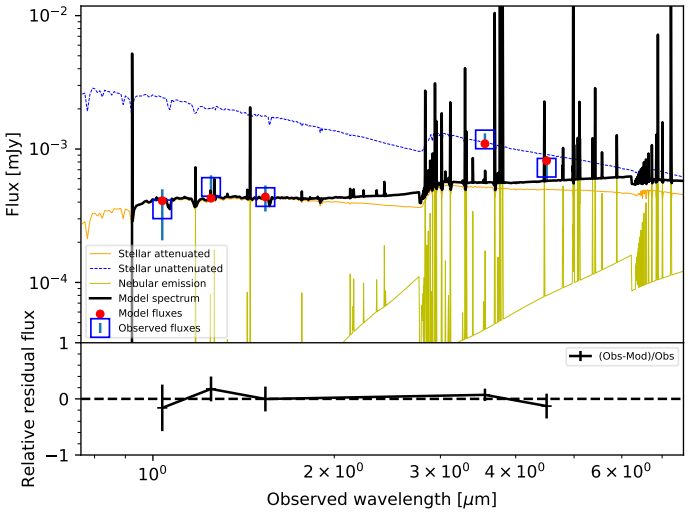

(ID67)

Fig. Set 1. SED Models of the 43 galaxies

Figure 1. The best-fit SED models of the 43 galaxies created using CIGALE (Boquien et al. 2019). The blue boxes are the observed fluxes while the red circles are the model fluxes. In general, the models are able to fit the observations, providing meaningful constraints on the extinction, UV slope β, and escape fraction. Furthermore, the models produce redder implied slopes than J20.

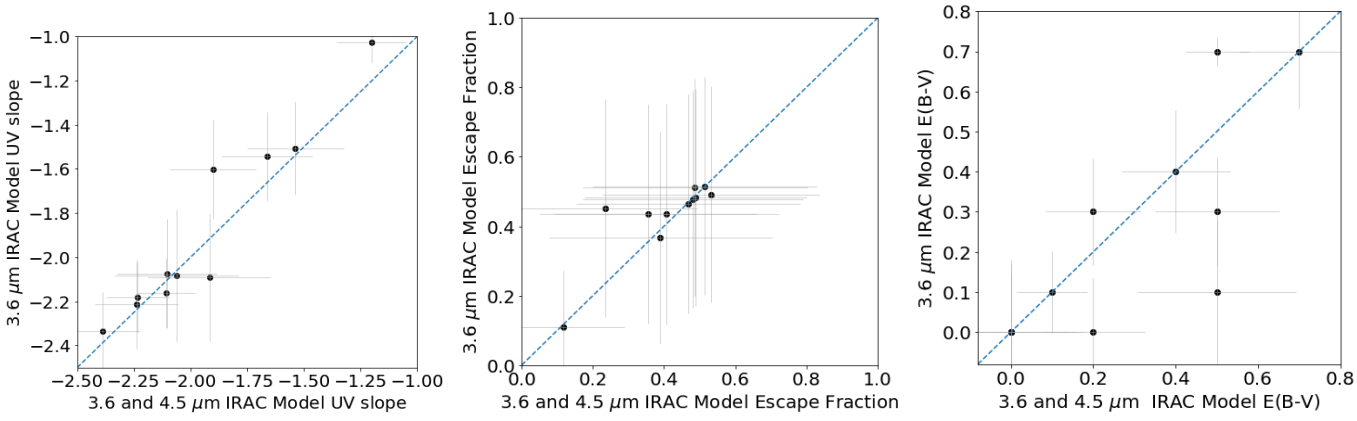

(d) (e) (f)

Figure 2. Comparison of β, $f_{\rm esc}$, and $E_{\rm B-V}$ of the models fit when both 3.6 and 4.5μm IRAC filters are included and when only 3.6μm is included, using the data of Tables 2 – 3. Only minor differences can be seen in the two sets of models, showing that the addition of the noisier IRAC2 4.5 μm data points does not affect the modeling greatly.

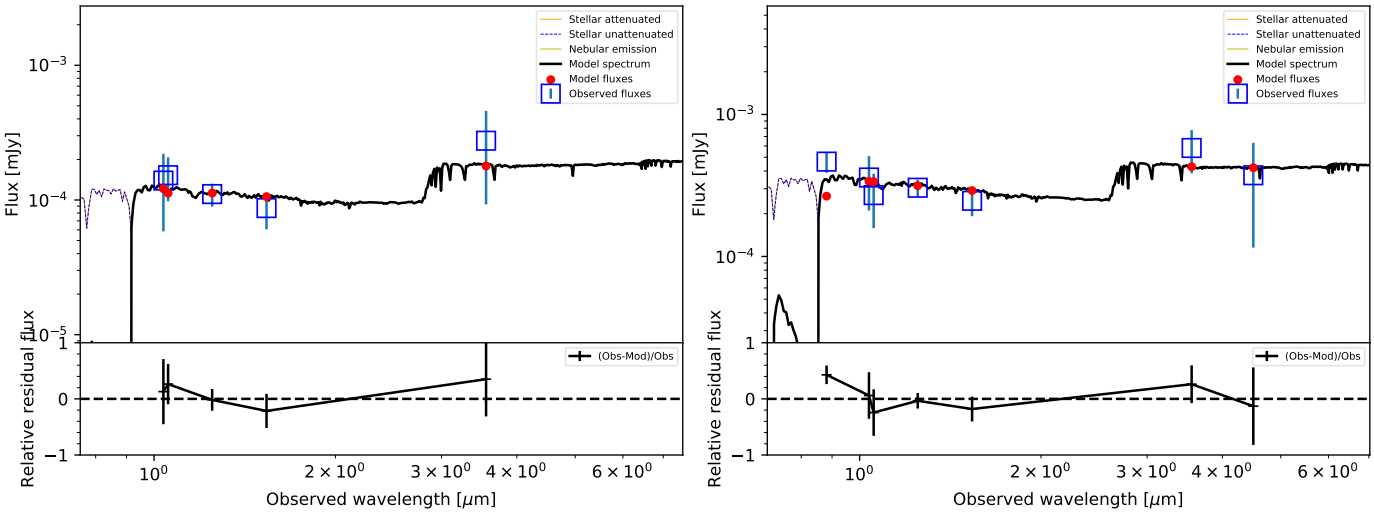

(m) (n)

Figure 3. The SED models fit with a fixed escape fraction of 1 for ID43 and ID63. **The models clearly show worse fits than in the corresponding panels of Fig. 1. Thus, the $f_{\rm esc}$ directly affects the fitting of the models.**

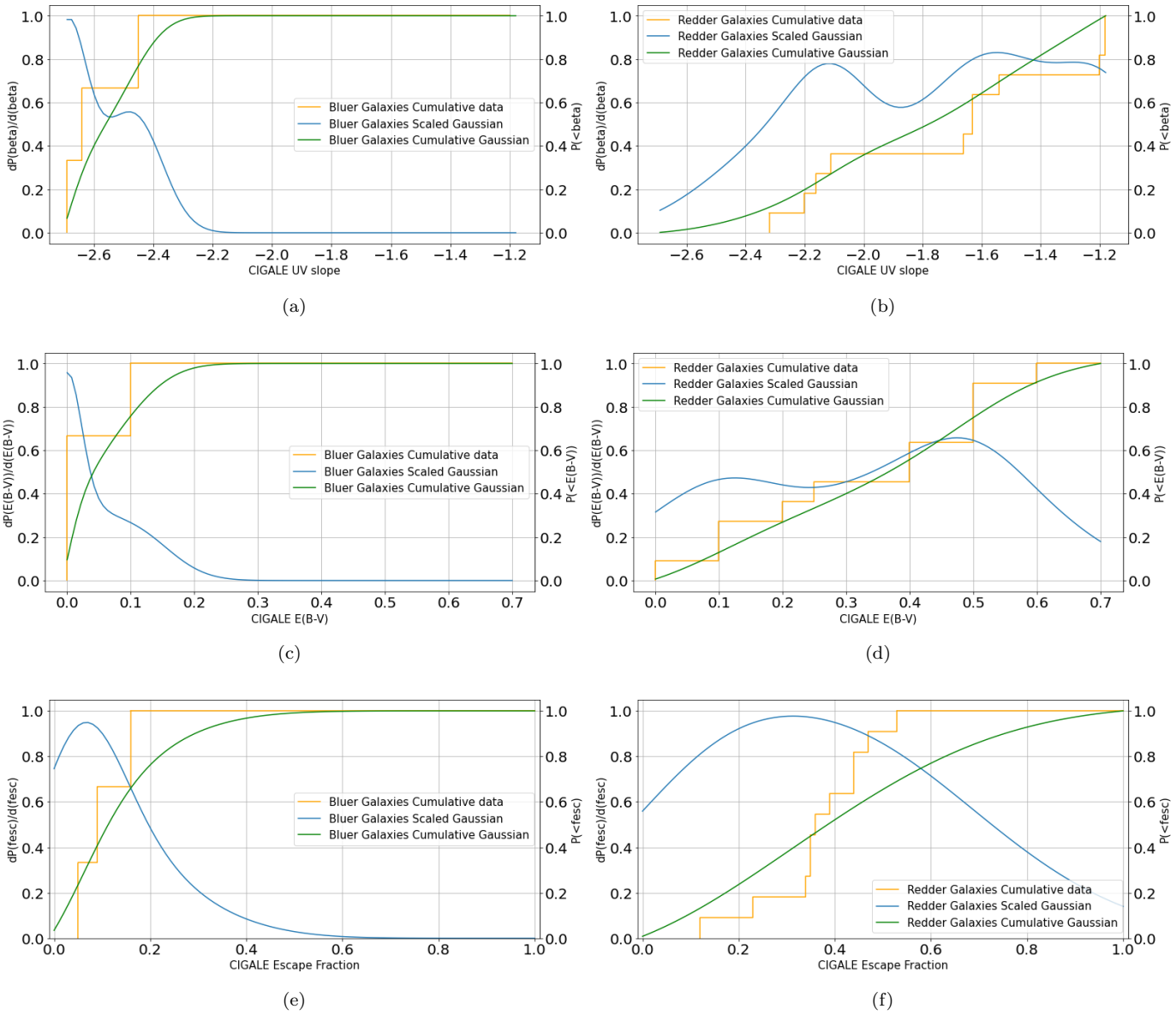

Figure 4. Distributions of the implied Bayesian UV slope and escape fraction, and best-fit $E_{\mathrm{B-V}}$ lines of the 14 galaxies that showed correlation between f_{esc} and their χ^2 fit. The sample is divided between bluer galaxies with model $\beta < -2.35$ and redder galaxies with model $\beta > -2.35$. The orange lines show the cumulative distributions of the individual adopted values with the probability shown on the right axis. The blue and green lines respectively show the scaled stacked model likelihoods and stacked cumulative distributions with probability for the latter on the left axis, assuming that the likelihood of the model parameter is normally distributed with the given mean and standard deviation. The plots show that bluer galaxies are more likely to have lower values of f_{esc} and lower $E_{\mathrm{B-V}}$.

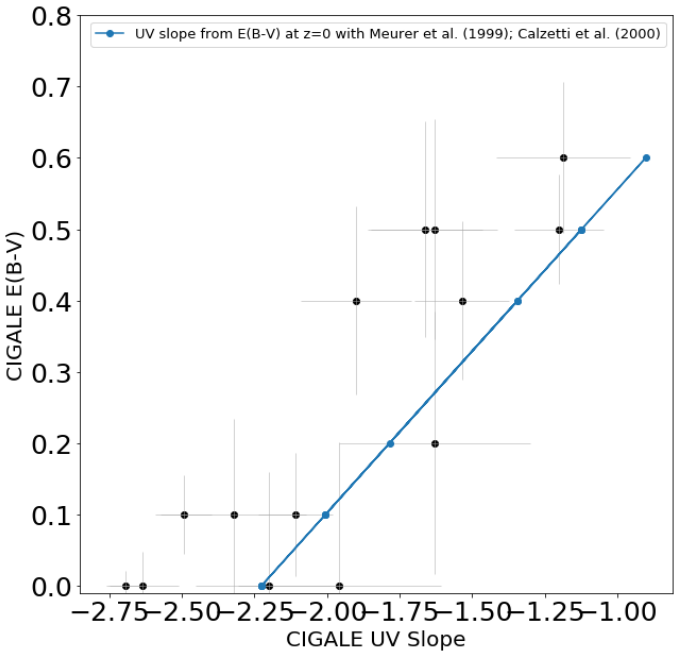

(a)

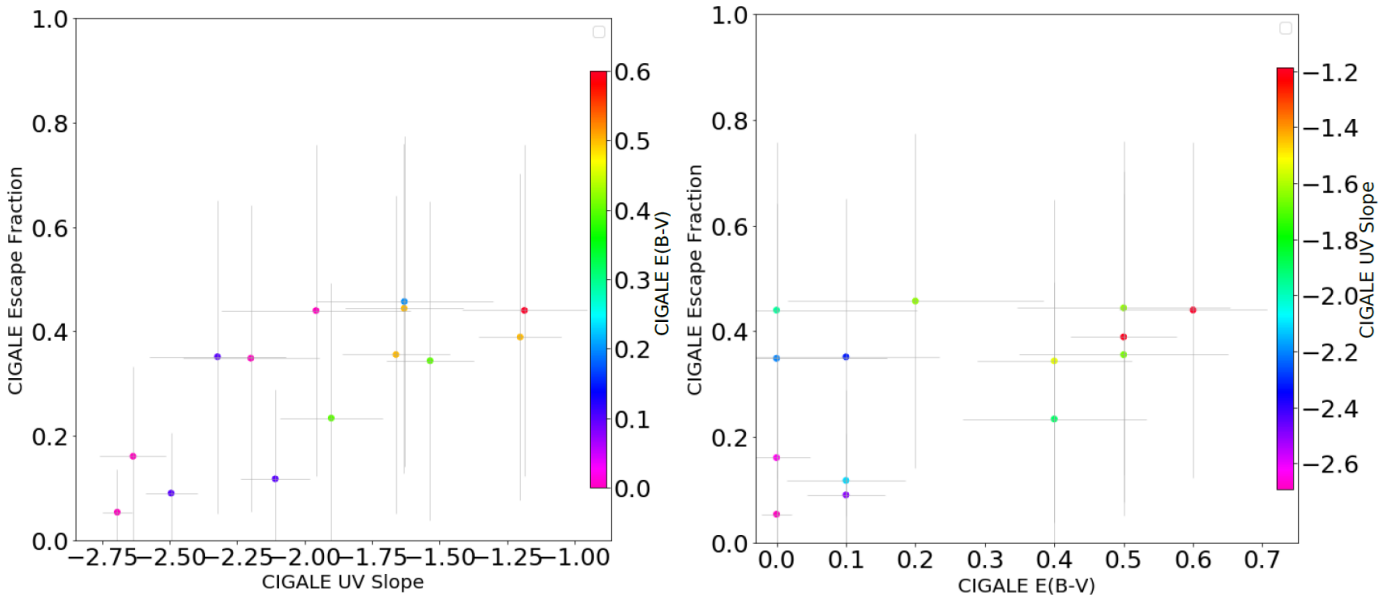

(b) (c)

Figure 5. plots showing the distributions of **Bayesian** β **and** $f_{\rm esc}$**, and best-fit** $E_{\rm B-V}$ **against each other for 14 galaxies that showed correlation between all its model** χ^2 **values and the difference between each model's best-fit and Bayesian** $f_{\rm esc}$. Fig. 5a shows that the implied β tends to be steeper (bluer) for lower implied $E_{\rm B-V}$ values. The local relation between $E_{\rm B-V}$ and β from Calzetti et al. (2000); Meurer et al. (1999) is plotted in blue, showing shallower β-values at $z \simeq 0$ compared to our SDF sample at $z \simeq 6$. Fig. 5b shows the trends between CIGALE model $f_{\rm esc}$ values and β, with the points color coded by their CIGALE $E_{\rm B-V}$ value: lower implied $f_{\rm esc}$ values are more probable at bluer CIGALE β **and** $E_{\rm B-V}$. Fig. 5c suggests that lower implied $f_{\rm esc}$ **and** β**-values** are somewhat more likely at lower CIGALE $E_{\rm B-V}$ values. Fig. 5b and c suggest that high nebular emission can lead to lower $f_{\rm esc}$ values. Since the LyC radiation of younger, bluer, and less dusty stellar populations goes into producing nebular emission instead, older, redder and somewhat dustier stellar populations may succeed better in letting more LyC radiation escape via holes vacated in the ISM by supernovae and/or weak AGN somewhat later in their evolutionary stage.